KERNFORSCHUNGSANLAGE JÜLICH GmbH
Institut für Kernphysik

Intranuclear Cascade Evaporation Model Predictions of Double Differential A(p,xn) Neutron Cross Sections and Comparison with Experiments at 318 MeV and 800 MeV Proton Energy

by

P. Cloth, P. Dragovitsch, D. Filges, Ch. Reul
and
W.B. Amian, M.M. Meier

Jül-2295
August 1989
ISSN 0366-0885

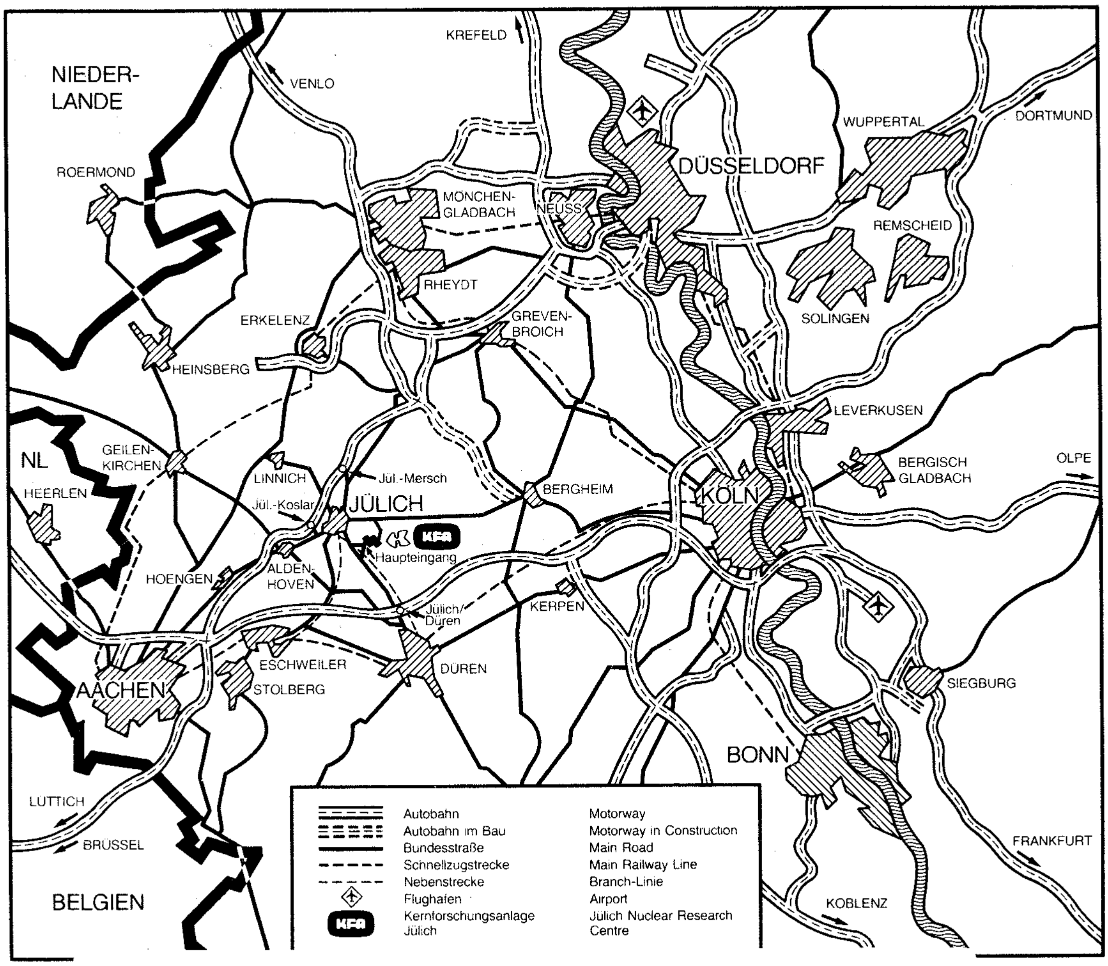

Berichte der Kernforschungsanlage Jülich – Nr. 2295
Institut für Kernphysik Jül-2295

Zu beziehen durch: ZENTRALBIBLIOTHEK der Kernforschungsanlage Jülich GmbH
Postfach 1913 · D-5170 Jülich (Bundesrepublik Deutschland)
Telefon: 02461/610 · Telex: 833556-0 kf d

Intranuclear Cascade Evaporation Model Predictions of Double Differential A(p,xn) Neutron Cross Sections and Comparison with Experiments at 318 MeV and 800 MeV Proton Energy

by

P. Cloth, P. Dragovitsch, D. Filges, Ch. Reul
and
W.B. Amian, M.M. Meier*

*Los Alamos National Laboratory, P.O. Box 1663,
Los Alamos NM 87545, USA

Table of Contents

1. Introduction

The intranuclear-cascade evaporation model (INCE) as implemented in the high energy radiation transport code HETC, subsystem of HERMES (1) is used in the calculation of double differential cross sections of proton induced neutron production. The investigations were done on target elements C, Al, Ta, Ni, W, Pb, and U at 318 MeV incident proton energy and on C, Al, Pb, and U at 800 MeV, respectively. The predictions of the INCE model were compared with experimental data for double differential cross sections taken at 7.5 and 30 degrees scattering angles at the Los Alamos WNR facility utilizing the Time of Flight (ToF) technique at LANL.The calculations performed here are part of a experimental-theoretical program within the LANL-KFA collaboration concerning medium energy cross section measurements mainly neutrons and state of the art computer code validations of these measurements. In general, the model predictions reproduce the correct neutron production for evaporation neutrons and are also in good agreement with the experimental data at high neutron energies. In the energy range dominated by preequilibrium processes an underestimation of experimental yields has to be remarked.

2. Calculational Model

The intranuclear cascade evaporation model was used as implemented in the high energy nucleon meson transport code HETC developed at ORNL (2). In the last few years various code modifications of HETC have been made at the Kernforschungsanlage Jülich (KFA) (3,4). All the modifications relevant to the included nuclear models refer to the evaporation model which involves the Eving-Weisskopf formalism (5) without a contribution from preequilibrium processes. The changes contain an update of the atomic masses using the 1977 Atomic Mass Evaluation values of Wapstra and Bos (6). The range of possible residual nuclei was extended by implementing the semiempirical mass formula of Cameron (7) in case of masses being not covered by those tables. Furthermore the parameter B_0 in the formula of the level density parameter is allowed to vary with A, using data compiled by Baba (8). A new kinematic calculation involving the recoil momentum of the residual nucleus allows non isotropic evaporation. At last the high energy fission model (RAL-model, (9)) has been included to the evaporation model based on the statistical model of Fong (10). In the actual update this modified HETC has been implemented into the framework of the HERMES code system (1), resulting in the actual version HETC/KFA-2. This code is coupled off-line by standardized HERMES submission files with additional Monte Carlo codes, each of these codes solving a specific part of the general problem. All codes are served by an unique command language (CMD) and use the same 3-dimensional geometric description (Combinatorical Geometry, CG). In addition an on-line analysis subroutine package (SIM) is adapted to each Monte Carlo code. SIM is used to provide the scoring of the physical results of the respective runs. A detailed description of the HERMES code system and of all modifications in HETC/KFA-2 even those relevant to the extranuclear algorithm of the code is given by Cloth et al. (1).

3. Calculational Procedure

3.1 Nuclear Models of the Set-Up

Performing HETC/KFA-2 model calculations the incident particles are selected uniformely over the geometric cross section of the nucleus. The intranuclear cascade model generally assumes that the interactions of high-energy particles with a nucleus can be represented by free-particle collisions inside the nucleus (intranuclear cascade), because the wave length of the incident particle is in the order of the internucleon distances. These collisions can be calculated by using elastic and inelastic nucleon-nucleon cross sections, pion-nucleon elastic scattering, charge exchange and pion production. When the particle energy becomes relatively small, it is assumed, neglecting any preequilibrium processes, that this energy is equally distributed among all residual nucleons in the nucleus. The subsequent processes are described in terms of the evaporation model EVAP (1), there a reequilibration of the nucleus between the successive particle emission is assumed. If required, the high energy fission model (RAL) can also be connected at the end of intranuclear cascade. In the INC model the nucleon density inside the nucleus is approximated to the Fermi-type distribution proposed by Hofstadter (11) and is carried out by partitioning the nucleus into three regions of constant density. The outer radius of each region is chosen by solving for r the density function at values of 90%, 20%, and 1% of the central density. Consequently the outest radius, squared and multiplied with π gives the "geometric" cross section of the nucleus. Also the nucleon momenta are assumed to be Fermi distributed and they are normalized for each region of nucleon density, while the potential energies of the nucleons are estimated as the sum of the zero temperatures of the nucleons and the binding energy of the most loosely bound nucleon.

3.2 Calculational Performance

The calculational predictions of proton induced neutron emission presented in this paper were made by using the so-called "thin target"-setup of HETC/KFA-2. In this set-up only the included nuclear models of HETC are taken into account. Starting an on-line analysis of emitted nucleons directly after their emission from the nucleus time consuming extranuclear transport algorithm are switched off. This procedure is somewhat different of previous published calculations (12) avoiding the writing of large event histories on computer storage devices. Physically this set-up can be understood as an ideal thin target consisting of only one nucleus. This method is valid because the "geometric" cross section of the bombarded nucleus is known by the code (1). This method results in significantly faster computing times than another method simulating the geometry of a real thin target used in experiments.

For U and Pb targets the RAL fission model (9) with a constant value of B_0=8 and an isotropic emission of secondary particles while evaporation in the laboratory system was used. For all other target nuclei the fission model was excluded and the variable B_0-option was selected while non-isotropic emission of evaporation particles was allowed. Depending on the number of emitted neutrons, in order to reach a good accuracy in the neutron yields the number of calculated histories varied between 250000 and 600000, requiring about 0.5 h cpu to 6.2 h cpu computer time on a IBM-3081 (see table II). The target material input data used in these tasks are given in table I. In order to keep optimal approximation to the available experimental data the same energy intervals for the on-line calculations were choosen like in the experimental setup described later. The angle intervals covered the whole range between 0 and 180 degree, whereby the experimental positions were specially taken into consideration. The energy- and the angle binning are given in table III. On this basis double-differential neutron yield spectra in units of neutrons per incident particle, $Y(\theta,E)$, were calculated with the HETC/KFA-2 code for every predefined energy-angle grid. To convert the calculated quantities into terms of double differential cross sections, these yield-spectra have to be normalized to the steradian of the respective angle-interval, to the size of the energy bin and last not least to the geometric cross section. In the opposite to recent versions of HETC the nuclear density of the target and its transparency must not be taken into account any longer (12). In this way the double differential cross section for neutron emission can be estimated as

$$d\sigma/(d\Omega \cdot dE) = Y(\theta,E) \cdot \Sigma_G/(d\Omega(\theta)\cdot\Delta E)$$

Comparisons of calculated and experimetal cross sections are commonly displayed in a double logarithmic scale using units of barns/(MeV·sr). But in this way it is nearly impossible to decide how the agreement between experiment and theory really is. For this reason we decided to represent the data in units of barns per unit lethargy and steradian. On this way discrepancies and agreements can be represented independent from energy in a true area kind. The respecting conversion is given by the relation:

$$\frac{d\sigma_i}{d\Omega \cdot dU} = \frac{d\sigma_i}{d\Omega \cdot dE} \cdot \frac{E_{i+1}-E_i}{\log E_{i+1}-\log E_i}$$

where $d\sigma_i/d\Omega dE$ is the double differential cross section in the energy interval $[E_i, E_{i+1}]$.

4. Neutron Cross Section Measurements

Only a brief description of the experimental method and of the off-line analysis to determinate double differential cross sections will be given here. A detailed discussion will be given by Meier et al. (13). The measurements were done at the low current target area of the LAMPF/WNR facility in Los Alamos/USA using the micropulse-structure of the accelerator for the time-of-flight technique. The cases studied were the same as described for the HETC/KFA-2 calculations above. Thin targets located in the center of the target area were bombarded with protons of 318 and 800 MeV kinetic energy in laboratory system, respectively. The thin targets were designed to make an energy loss less than 2 MeV. They were viewed by detectors positioned at a distance of 30 m at 7.5 degrees and of 40 m at 30 degrees. The energies of the neutrons were derived from their flight time between the passage of the proton burst through a time pick-off and the detector signal. For the absolute calibration of the time scale the arrival of the prompt gamma rays was used. Furthermore the corresponding pulse heigth was recorded for each event in order to allow software bias definition during data reduction. The emitted neutrons were collimated by a set of steel collimators positioned in the flight path at approximately 3 m away from the target defining a wider neutron beam than the detector cross section. Charged particles were partially removed from the neutron flight paths by a set of dipole magnets. The remaining charged particle flux was reduced by multiple scattering in a set of uranium absorbers. The residual background of charged particles arriving in the detector could finally be supressed electronically by operating a 0.3 cm thin additional plastic detector in front of the neutron detector in anticoincidence. The energy-dependent efficiencies of the neutron detectors were obtained by an intercomparison with a calibrated detector (14) in the same neutron flux. The attenuation of the neutron flux in air and aluminum was calculated by using ENDF (15) cross sections. For the uranium filters wrapped in polyethylene, the combined attenuation was measured by inserting various additional filters into the neutron flight path. For a detailed description see Ref. 13. Because of approx. 300 ps wide micropulses containing $2 \cdot 10^7$ protons and their highly instantaneous rate all time-of-flight spectra had to be corrected for the deadtime associated with the suppression of slow neutrons after the stop on the arrival of a fast one. Typical corrections were in the order of 10% for the lowest energies. The validity of the deadtime correction, the background estimation and of the charge normalization was checked by measuring the neutron transmission through graphite absorbers giving an agreement within 5% with ENDF data. An estimation of the uncertainties of the final differential cross sections - except the statistical ones - is given in table IV. There the energy resolutions estimated from the width of the gamma-flash are shown.

5. Comparison of HETC/KFA-2 Predictions with Experimental Results

The HETC/KFA-2 runs were analyzed not only at angle intervals corresponding to the experimental cases but over the whole range from 0. degree to 180 degree. In the present context only the two experimental angles of 7.5 and 30 degree, and the corresponding angle intervals at HETC/KFA-2 of 6-9 and 28.5-31.5 degrees will be discussed. For an overview, the energy- and angle- integrated neutron and proton yields of the HETC/KFA-2 calculations are given in table V. They show the typical increase of neutron- and proton production with increasing target mass. Also given are contributions of the individual nuclear models. The total cross section for neutron and proton production can be calculated by multipling these values by the respective geometric cross section given in table II. The explicite results of the calculations are given in Appendix C. The experimental data are available at NNDC (16, see also 13).

In figs. 1 - 22 the cross sections calculated with HETC/KFA-2 are compared with the measurements described above. In these representations all data are given in units of barns per unit lethargy and steradian making a dircect comparision possible. The calculated cross sections are plotted as histograms. Their typical statistical uncertainties are in the order of 5-20% (one standard deviation), except for a few energy groups. The results of the measurements are displayed as circles. For a better comparability only their statistical uncertainties were taken into account in the figures. To estimate their total uncertainties one has to add the values given in table IV using the methods for error propagation.

5.1 318 MeV Incident Energy

At an incident energy of 318 MeV a good agrement between HETC-predictions and measurements can be observed in the energy range where evaporation processes are assumed. In case of emission at 7.5 degree the energy range where both agree depends on the target mass. It reaches to 50 MeV for C and Al and decreases with greater masses (U, Pb) down to the order of 20 MeV. This effect is not observed at 30 degrees. There the cross sections are well approximated up to 20 MeV, independent on the target material. For neutron energies close to the projectile energy a quite good prediction of the measurements can be remarked. The peak resulting from quasi elastic scattered neutrons is reproduced in all cases and shows a good quantitative agreement especially for heavy targets at 7.5 degrees and for light and medium targets at 30 degrees. Systematically the quasi-elastic peak observed in the measurements has its maximum at somewhat lower energies than the ones predicted by the HETC. Unfortunately the range of preequilibrium processes cannot be reproduced correctly by the computer simulation. At energies above about 20 MeV and, up to 250 MeV, the code underestimates the cross sections by a factor of two or more.

5.2 800 MeV Incident Energy

Like for 318 MeV at 800 MeV the double differential cross sections for neutron emission are well described by HETC at evaporation regions. Surprising is the excellent approximation for light targets up to about 200 MeV at 7.5 degrees and up to 50 MeV at 30 degrees, respectively. For higher neutron energies the neutron emission is systematically underestimated by the used model, while the quasi elastic peak is overestimated. At 30 degree emission the measurements show no peak for high energies while the calulation predicts one. For heavy targets HETC/KFA-2 code is in good agreement with the ToF-measurements up to 300-400 MeV. The emission of quasi elastic scattered neutrons is also well reproduced. The energy range inbetween is as in the case of 318 MeV incident energy underestimated by the simulation at 7.5 degrees. On the other hand at 30 degree the neutron emission from heavy targets is given in an excellent manner by HETC in this range.

6. Conclusions

The accuracy of HETC/KFA-2 code calculations has been tested for thin target neutron production by 318 MeV and 800 MeV incident proton energy, respectively, at two discret angles (7.5 and 30 degree). The Code is able to predict differential neutron production cross sections over the whole evaporation region for all target elements with a good accuracy. In the cascade region the code predictions are less sufficient. In this range it systematically underpredicts the experimental spectra by a factor of two and more. These systematic discrepancies between measurements and model predictions are also found and mentioned in Ref. (12). The dependence on the target mass of energy-integrated cross sections providing information about the nuclear reaction mechanism is demonstrated. In the energy range dominated by preequilibrium processes on underestimation of experimental yields has also to be remarked.
An extension of the INCE model by a nuclear model describing the hadron emission for preequilibrium processes could remove these discrepancies.

References:

(1) P. Cloth, D. Filges, R.D. Neef, G. Sterzenbach, Ch. Reul, T.W. Armstrong, B.L. Colborn, B. Anders, and H. Brückmann KFA-Report, Jül-2203, 1988

(2) K.C.Chandler and T.W.Armstrong, Oak Ridge National Laboratory Report ORNL-4744, 1972; Nucl. Sci. Eng. 49, 110 (1972).

(3) P.Cloth, D.Filges, G.Sterzenbach, T.W.Armstrong, and B.L.Colborn, Kernforschungsanlage Jülich Report Jül-Spez-196, 1983.

(4) T.W.Armstrong, P.Cloth, B.L.Colborn, D.Filges, and G.Sterzenbach, in Proceedings of ICANS VII, AECL Report AECL-8488, 1984, 205.

(5) V.F.Weisskopf, Phys. Rev. 52, 295, (1937); V.F.Weisskopf and H.D.Ewing, ibid. 50, 475 (1940)

(6) H.Wapstra and K.Bos, At. Data Nucl. Data Tables 19, 175 (1977)

(7) A.G.W.Cameron, Can. J. Phys. 35, 1021 (1957); 36, 1043 (1958)

(8) H.Baba, Nucl. Phys. A159, 625 (1970).

(9) F.Atchinson, in: Proceedings of the ICANS IV Meeting, KFA Jülich, 1979, KFA Report Jül-Conf-34, 1980, p.17.

(10) P.Fong, "Statistical Theory of Nuclear Fission", Gordon and Beach Science Publishers, New York, 1969.

(11) R.Hofstadter
Revs. Mod. Phys. 28, 214, (1956).

(12) D. Filges, P. Cloth, T.W. Armstrong, S. Cierjacks, Y. Hino F. Raupp, and L. Buth
Physical Review C, Vol. 36, No. 5, p. 1988-1994, Nov. 1987
(see also: Vol. 36, No. 5, p. 1976-1987)

(13) M.M.Meier, D.B.Holtkamp, G.L.Morgan, H.Robinson, G.J.Russell, E.R.Whitaker, W.Amian, N.Paul
submitted to: Phys. Rev. C.

(14) S.Howe, Nucl. Instr. Meth. 193 (1982), 565.

(15) D.I.Garber et al., BNL-325

(16) NNDC Compiled Neutron Emission Data
National Nuclear Data Center, Brookhaven Nat. Lab.,
Upton, NY 11973

Appendix A: Calculational and Experimental Quantities

Table I: Target Material Input Data

Target	Isotopes	Aboundance
C	^{12}C	98.9 %
	^{13}C	1.1 %
Al	^{27}Al	100 %
Ni	^{58}Ni	67.88 %
	^{60}Ni	26.23 %
	^{61}Ni	1.19 %
	^{62}Ni	3.66 %
	^{64}Ni	1.08 %
Ta	^{180}Ta	0.0123%
	^{181}Ta	99.9877%
W	^{180}W	0.135 %
	^{182}W	26.41 %
	^{183}W	14.4 %
	^{184}W	30.64 %
	^{186}W	28.41 %
Pb	^{206}Pb	27.7 %
	^{207}Pb	20.8 %
	^{208}Pb	51.5 %
U	^{235}U	0.212 %
	^{238}U	99.788 %

Table II: Geometric cross section, transparency and number of events for various target masses

Proton Energy (MeV)	Target Element	"Geometric" Cross-Sect. (b)	Transparency of the Nucleus	CPU per source proton (ns)	Source events calculated
318	C	0.7745	0.721	3.8	$5\cdot10^5$
800	C	0.7745	0.636	5.3	$5\cdot10^5$
318	Al	1.0282	0.614	7.0	$5\cdot10^5$
800	Al	1.0282	0.523	10.8	$5\cdot10^5$
318	Ni	1.3984	0.519	12.8	$6\cdot10^5$
318	Ta	2.3043	0.366	29.3	$4\cdot10^5$
318	W	2.3214	0.365	29.6	$4\cdot10^5$
318	Pb	2.4572	0.353	31.1	$2.5\cdot10^5$
800	Pb	2.4572	0.295	57.9	$2.5\cdot10^5$
318	U	2.6262	0.338	34.9	$2.5\cdot10^5$
800	U	2.6262	0.283	89.0	$2.5\cdot10^5$

Table III: Angle- and Energy Grids used in the HETC/KFA-2 Calculations

a) Angle Grids (degree):

0	1	2	3	6	9
12	15	18	21	24	27
28.5	31.5	33	36	39	42
45	48	51	54	57	60
63	66	69	72	75	78
81	84	87	90	93	96
99	102	105	108	111	114
117	120	123	126	129	132
135	138	141	144	147	150
153.5	156	159	162	165	168
171	174	177	180		

b) Energy Grids (MeV):

800	775	725	675	625	575	525
490	470	450	430	410	390	370
350	330	310	290	270	250	230
210	195	185	175	165	155	145
135	125	115	105	97.5	92.5	87.5
82.5	77.5	72.5	67.5	62.5	57.5	52.5
49	47	45	43	41	39	37
35	33	31	29	27	25	23
21	19.5	18.5	17.5	16.5	15.5	14.5
13.5	12.5	11.5	10.5	9.75	9.25	8.75
8.25	7.75	7.25	6.75	6.25	5.75	5.25
4.75	4.0	3	3	1.5	1	0.8
0.6	0.4	0.3	0.2	0.15	0	

Table IV: Estimated Experimental Uncertainties

a) Uncertainties in Double Differential Cross Sections except Statistical ones

Angle (degree)	Energy Range E_n<30MeV	30MeV<E_n<150MeV	150MeV<E_n<650MeV	650MeV<E_n<800MeV
7.5	12%	15%	17%	19%
30	10.5%	13.5%	15.5%	17.5%

b) Energy Resolution*

Angle (degree)	Neutron Energy 800 MeV	318 MeV
7.5	5%	2.5%
30	7%	3%

*estimated from the width of the gamma flash

Table V: Total proton and neutron yields calculated with HETC/KFA-2

	p-energy [MeV]	target	total n-yield	total p-yield	n/p total	neutrons from INC	protons from INC	n/p INC	n/p EVAP
1	318	C	0.336	0.628	0.535	0.269	0.477	0.564	0.443
2	318	Al	0.705	1.018	0.692	0.473	0.713	0.663	0.761
3	318	Ni	1.312	1.823	0.719	0.727	0.989	0.735	0.701
4	318	Ta	5.537	0.990	5.593	1.301	0.797	1.632	21.9
5	318	W	6.633	0.997	6.653	1.310	0.797	1.644	26.6
6	318	Pb	5.055	0.844	5.989	1.353	0.723	1.871	29.9
7	318	U	7.580	0.845	8.970	1.436	0.698	2.057	41.8
8	800	C	0.630	0.958	0.658	0.500	0.752	0.665	0.631
9	800	Al	1.443	1.723	0.837	0.937	1.199	0.781	0.966
10	800	Pb	9.124	1.988	4.589	2.765	1.525	1.813	13.7
11	800	U	13.45	2.623	5.128	3.023	1.621	1.865	10.4

Appendix B

In figs. 1-22 the double differential cross sections calculated with HETC/KFA-2 are compared with the time-of-flight measurements. All data are given in units of barns per unit lethargy and steradian. The calculated cross sections are plotted as histograms. The experimental data are displayed as circles, taking into account only their statistical uncertainties.

List of figures:

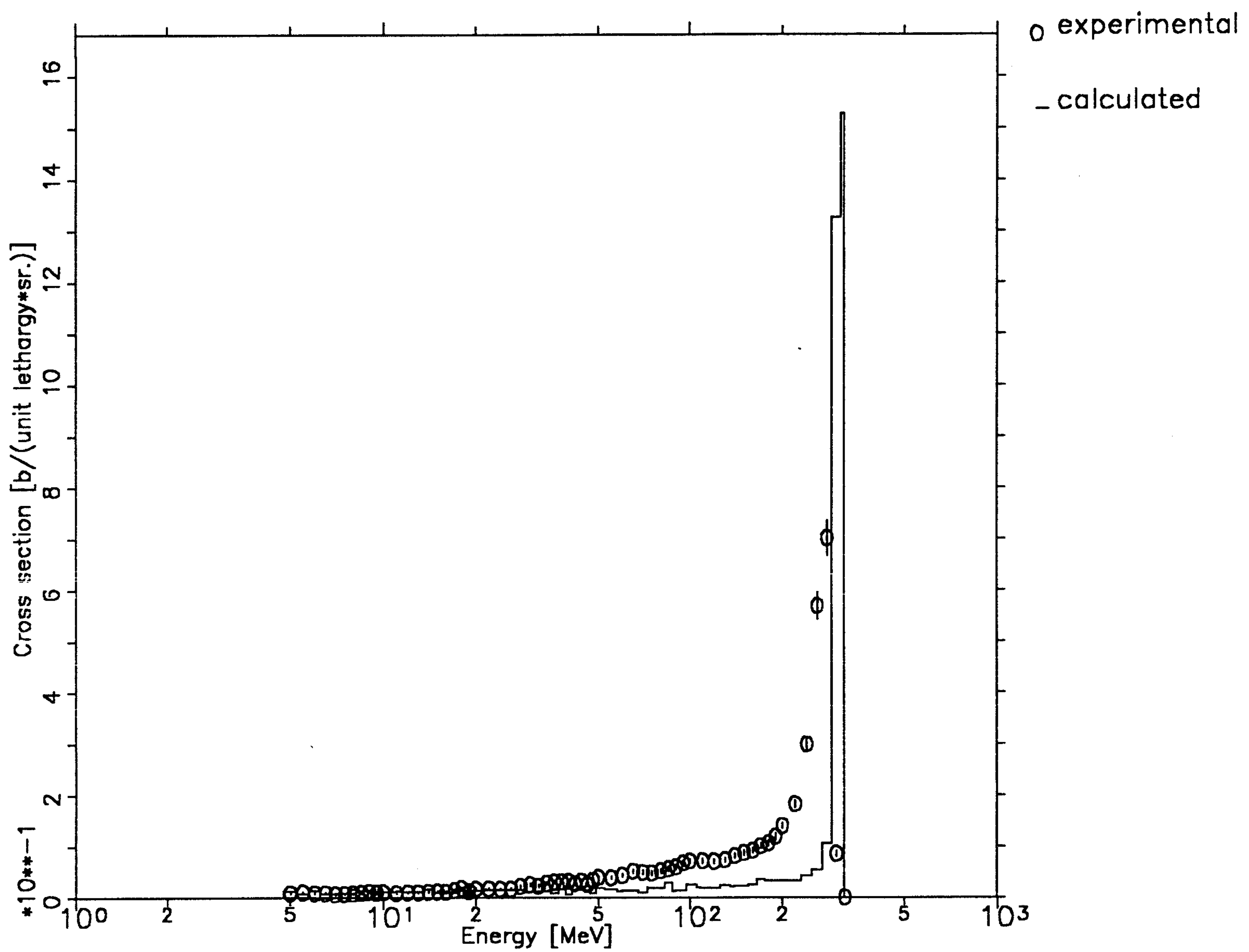

Fig.1: cross section for neutron emission at 7.5 deg from C bombarded with 318 MeV protons:
Comparision of ToF—measurements and HETC—calculations

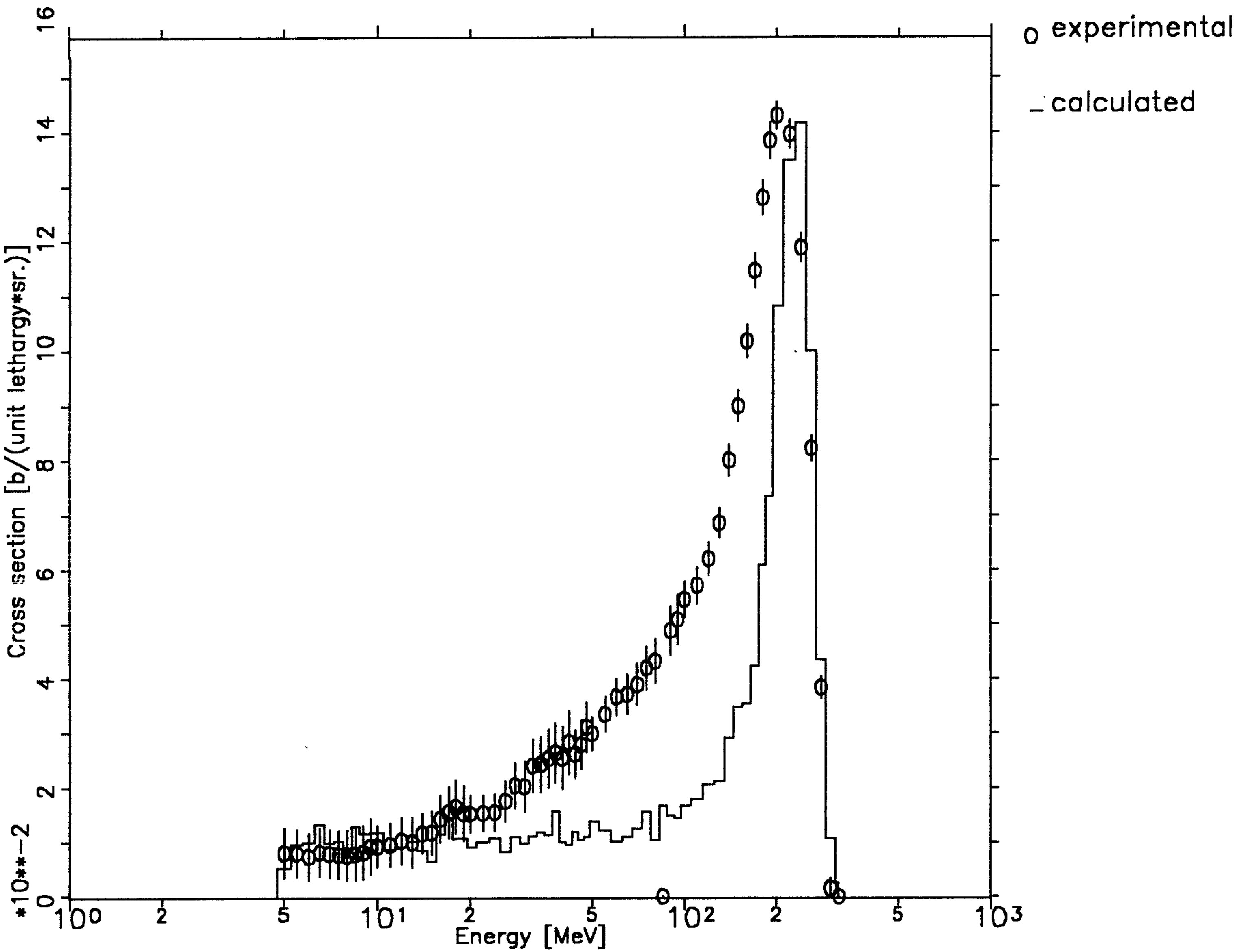

Fig.2: Cross section for neutron emission at 30. deg from C bombarded with 318 MeV protons:
Comparision of ToF–measurements and HETC–calculations

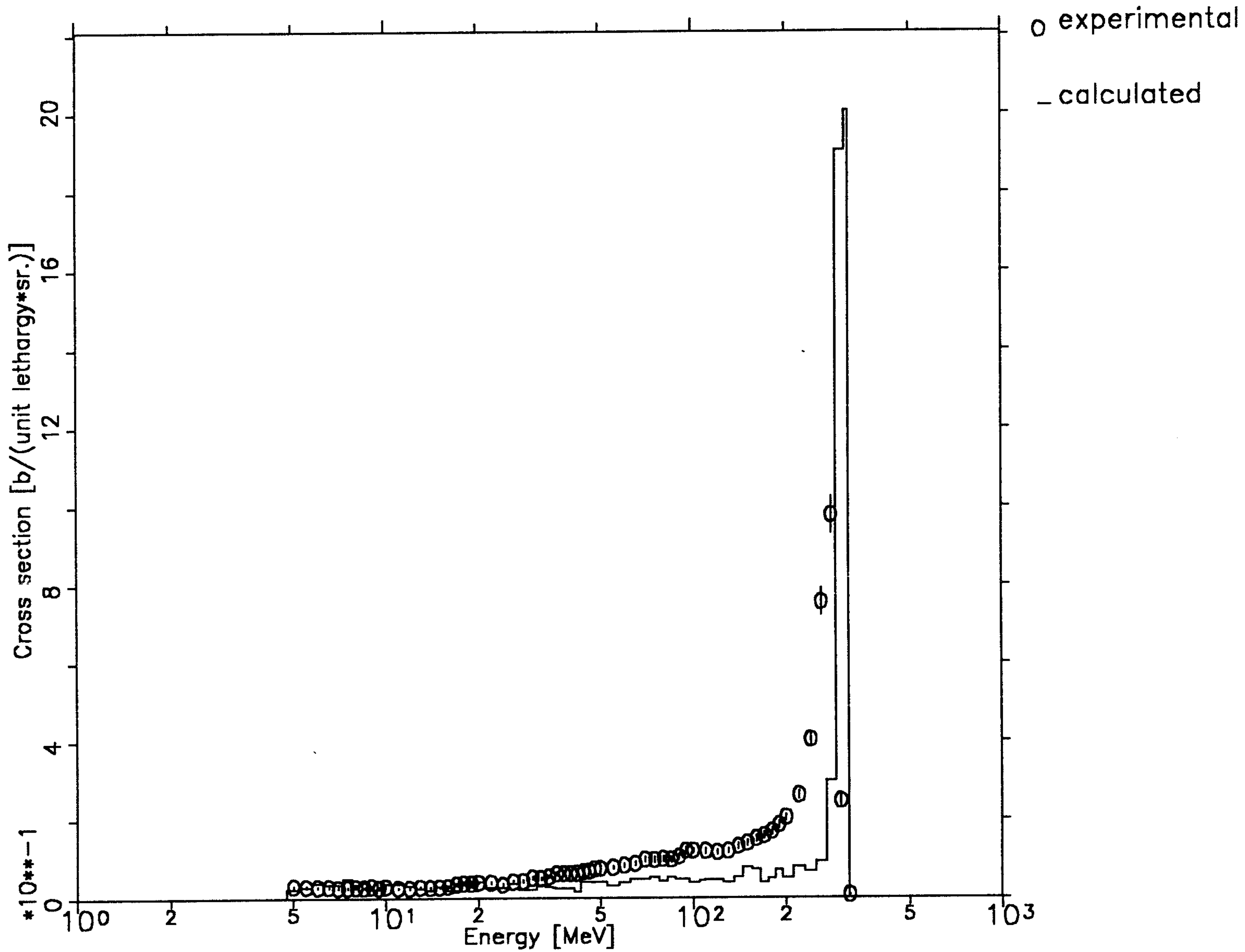

Fig. 3: cross section for neutron emission at 7.5 deg from Al bombarded with 318 MeV protons:
Comparision of ToF–measurements and HETC–calculations

1. Introduction

The intranuclear-cascade evaporation model (INCE) as implemented in the high energy radiation transport code HETC, subsystem of HERMES (1) is used in the calculation of double differential cross sections of proton induced neutron production. The investigations were done on target elements C, Al, Ta, Ni, W, Pb, and U at 318 MeV incident proton energy and on C, Al, Pb, and U at 800 MeV, respectively. The predictions of the INCE model were compared with experimental data for double differential cross sections taken at 7.5 and 30 degrees scattering angles at the Los Alamos WNR facility utilizing the Time of Flight (ToF) technique at LANL.The calculations performed here are part of a experimental-theoretical program within the LANL-KFA collaboration concerning medium energy cross section measurements mainly neutrons and state of the art computer code validations of these measurements. In general, the model predictions reproduce the correct neutron production for evaporation neutrons and are also in good agreement with the experimental data at high neutron energies. In the energy range dominated by preequilibrium processes an underestimation of experimental yields has to be remarked.

2. Calculational Model

The intranuclear cascade evaporation model was used as implemented in the high energy nucleon meson transport code HETC developed at ORNL (2). In the last few years various code modifications of HETC have been made at the Kernforschungsanlage Jülich (KFA) (3,4). All the modifications relevant to the included nuclear models refer to the evaporation model which involves the Eving-Weisskopf formalism (5) without a contribution from preequilibrium processes. The changes contain an update of the atomic masses using the 1977 Atomic Mass Evaluation values of Wapstra and Bos (6). The range of possible residual nuclei was extended by implementing the semiempirical mass formula of Cameron (7) in case of masses being not covered by those tables. Furthermore the parameter B_0 in the formula of the level density parameter is allowed to vary with A, using data compiled by Baba (8). A new kinematic calculation involving the recoil momentum of the residual nucleus allows non isotropic evaporation. At last the high energy fission model (RAL-model, (9)) has been included to the evaporation model based on the statistical model of Fong (10). In the actual update this modified HETC has been implemented into the framework of the HERMES code system (1), resulting in the actual version HETC/KFA-2. This code is coupled off-line by standardized HERMES submission files with additional Monte Carlo codes, each of these codes solving a

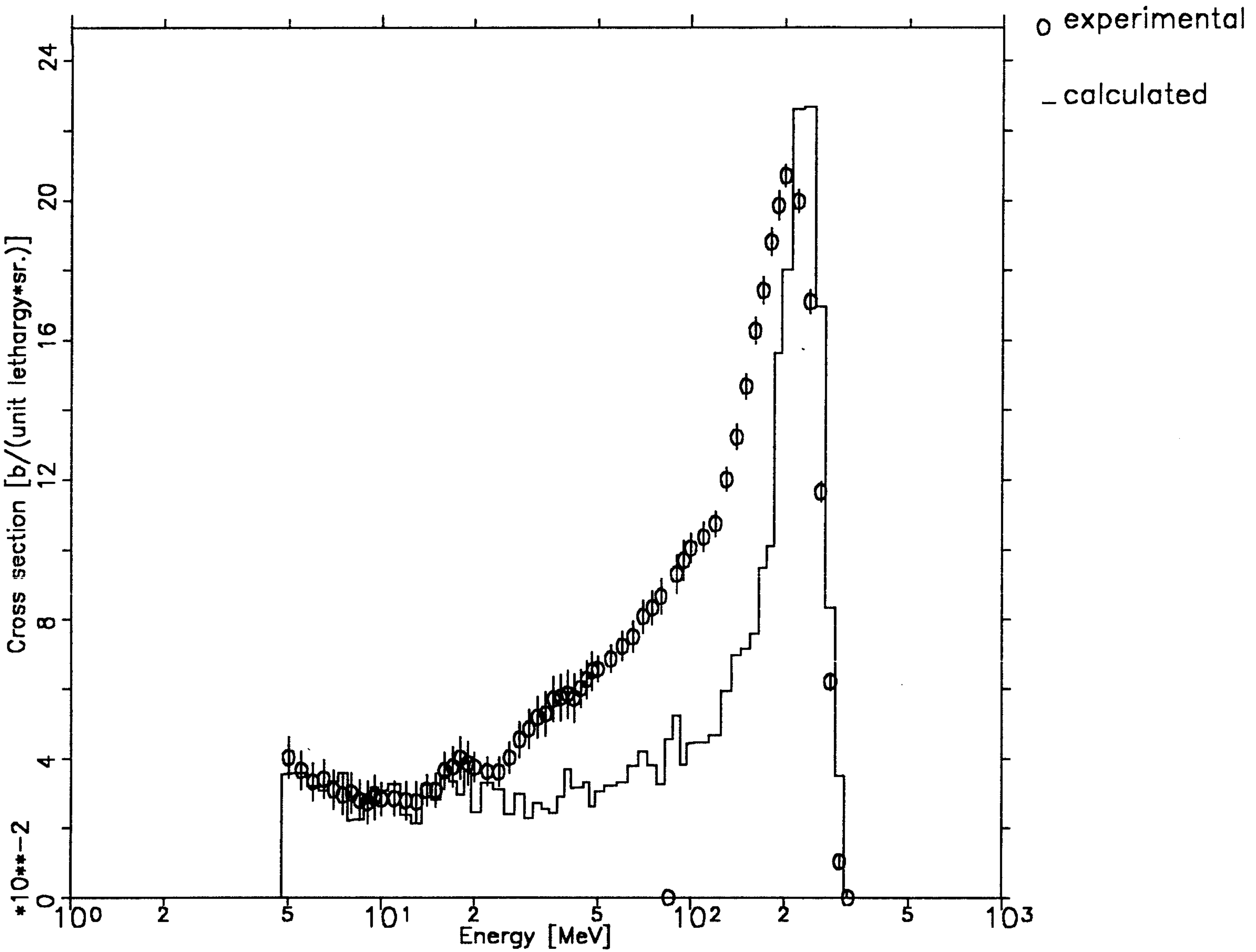

Fig. 4: Cross section for neutron emission at 30. deg from Al bombarded with 318 MeV protons:
Comparision of ToF–measurements and HETC–calculations

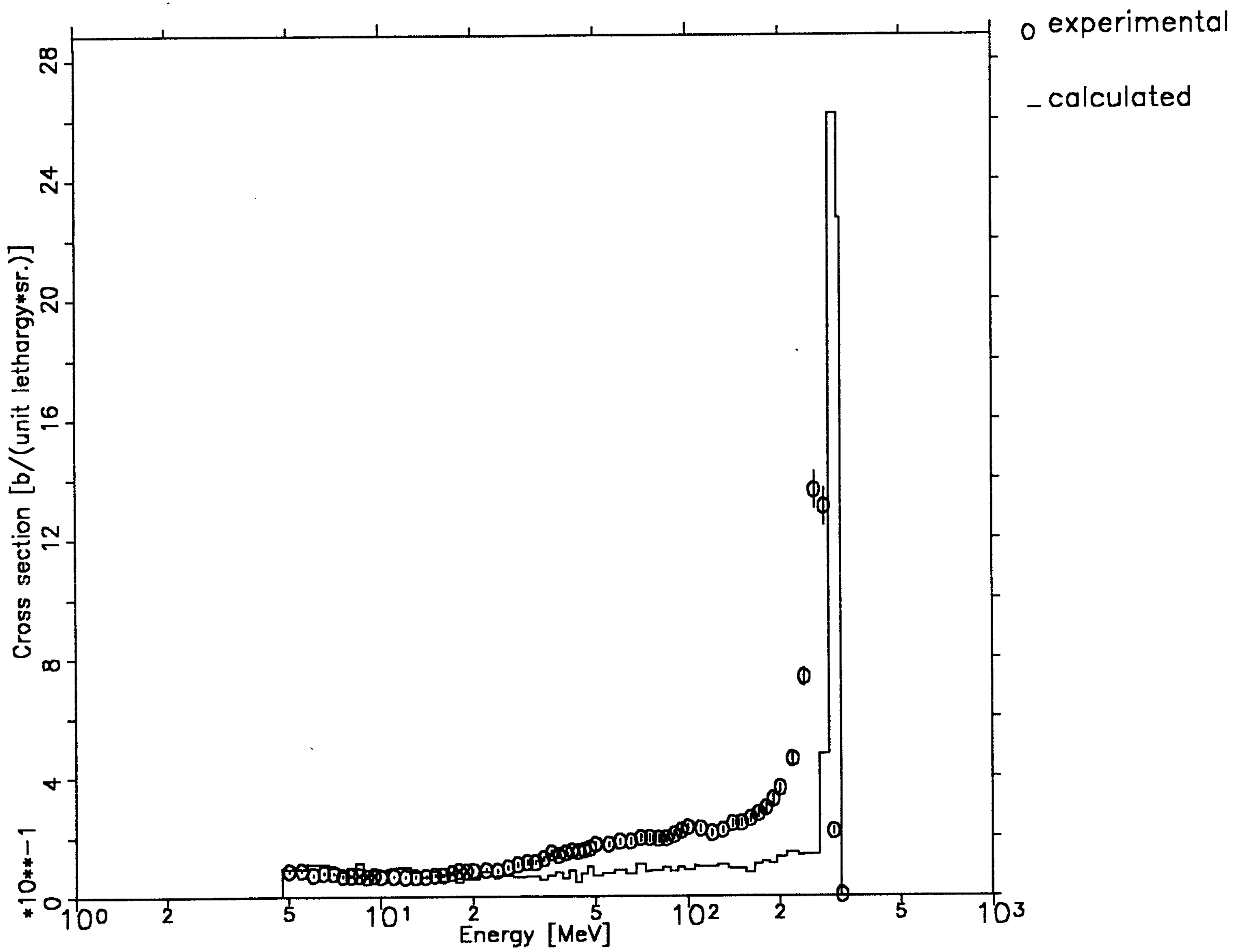

Fig. 5: cross section for neutron emission at 7.5 deg from Ni bombarded with 318 MeV protons:
Comparision of ToF—measurements and HETC—calculations

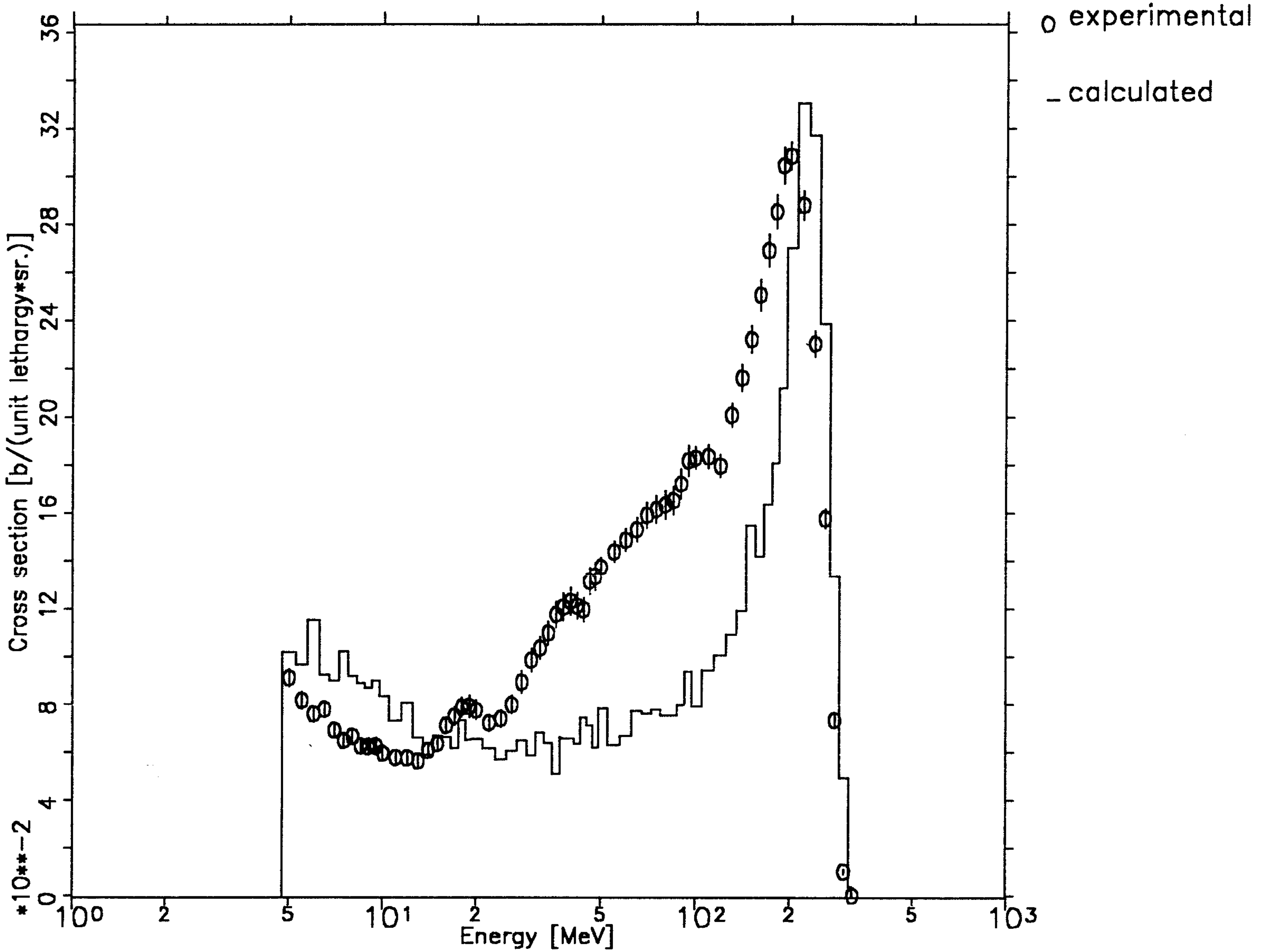

Fig.6: Cross section for neutron emission at 30. deg from Ni bombarded with 318 MeV protons:
Comparision of ToF—measurements and HETC—calculations

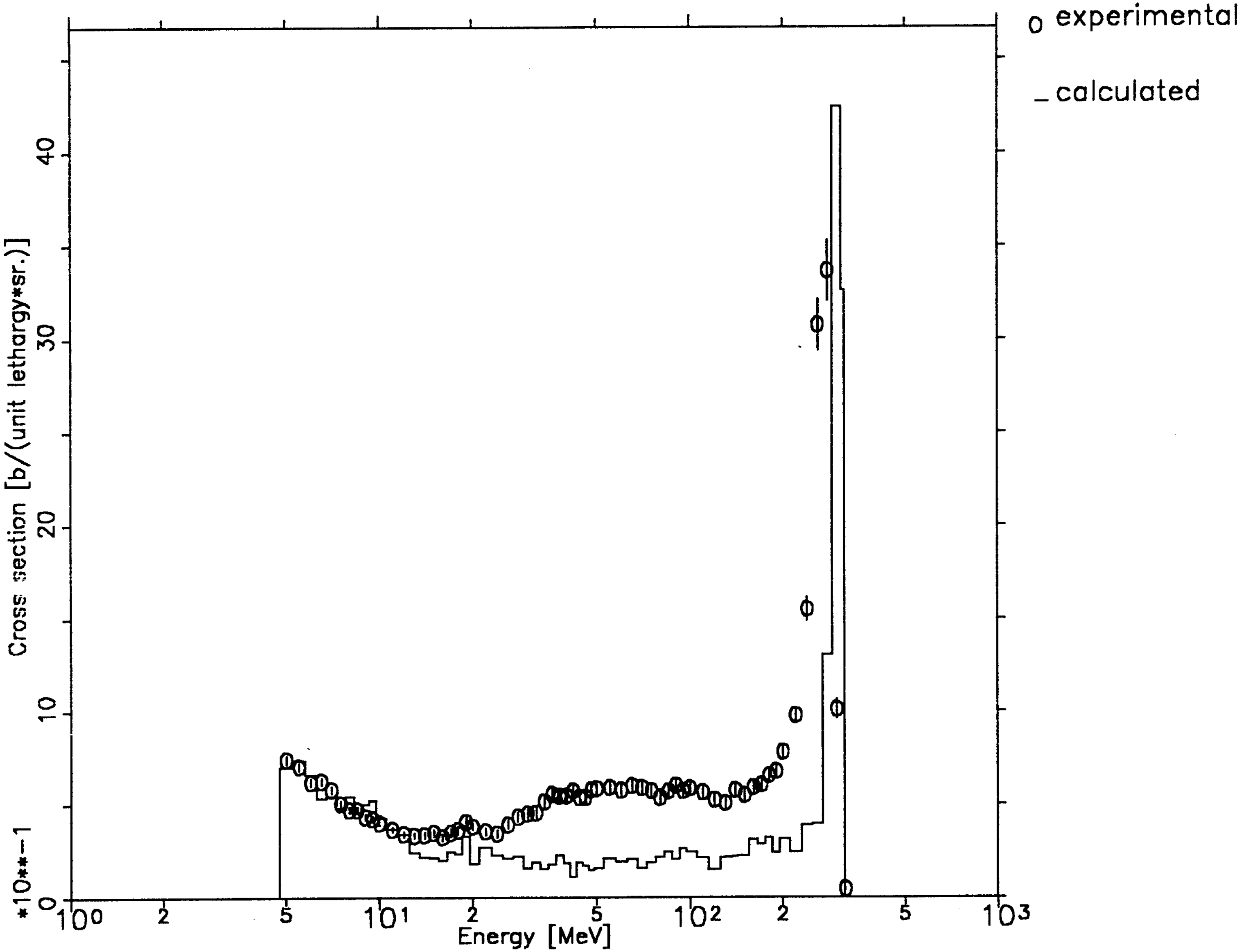

Fig. 7: cross section for neutron emission at 7.5 deg from Ta bombarded with 318 MeV protons:
Comparision of ToF-measurements and HETC-calculations

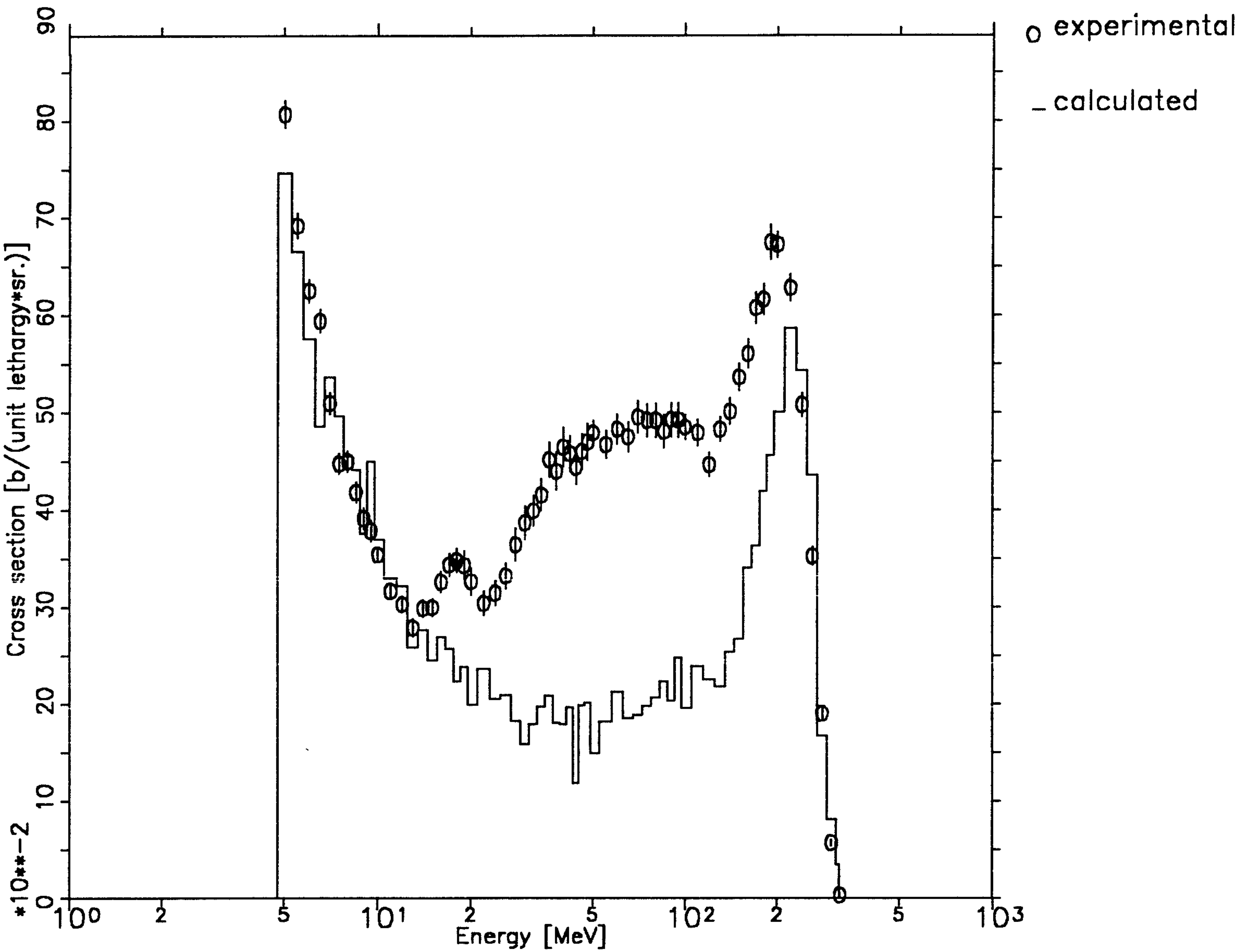

Fig. 8: Cross section for neutron emission at 30. deg from Ta bombarded with 318 MeV protons:
Comparision of ToF–measurements and HETC–calculations

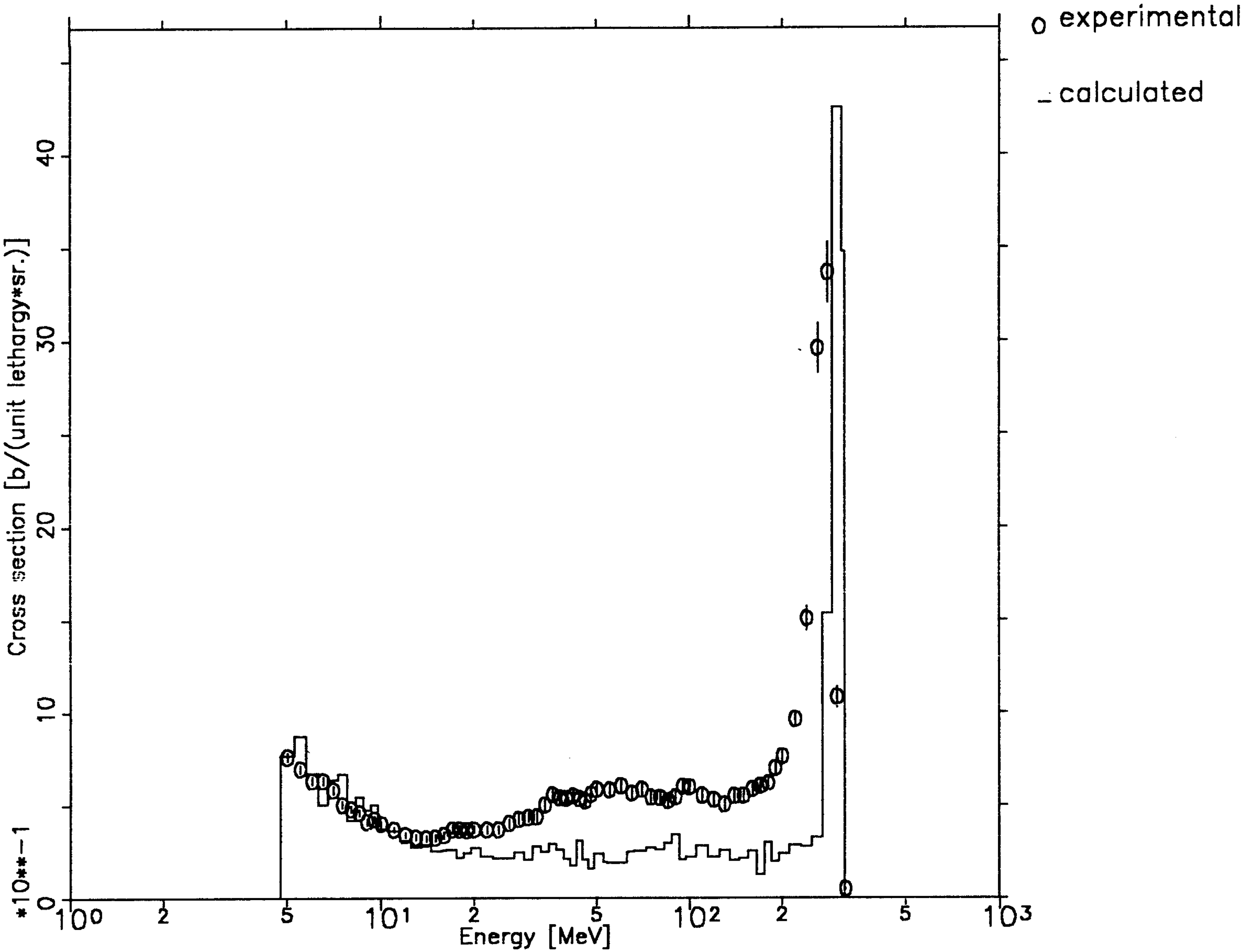

Fig. 9: cross section for neutron emission at 7.5 deg from W bombarded with 318 MeV protons:
Comparision of ToF—measurements and HETC—calculations

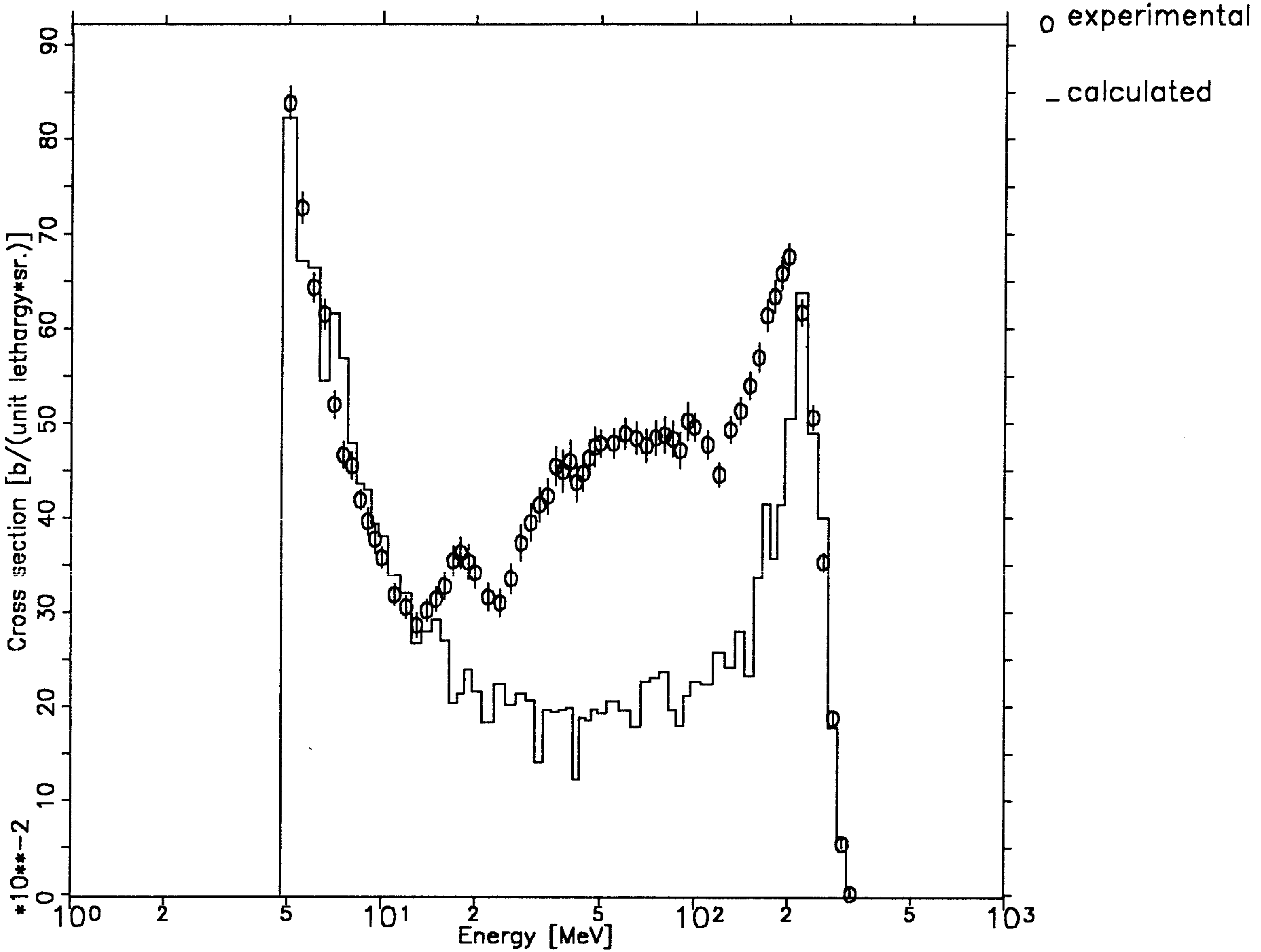

Fig. 10: Cross section for neutron emission at 30. deg from W bombarded with 318 MeV protons:
Comparision of ToF–measurements and HETC–calculations

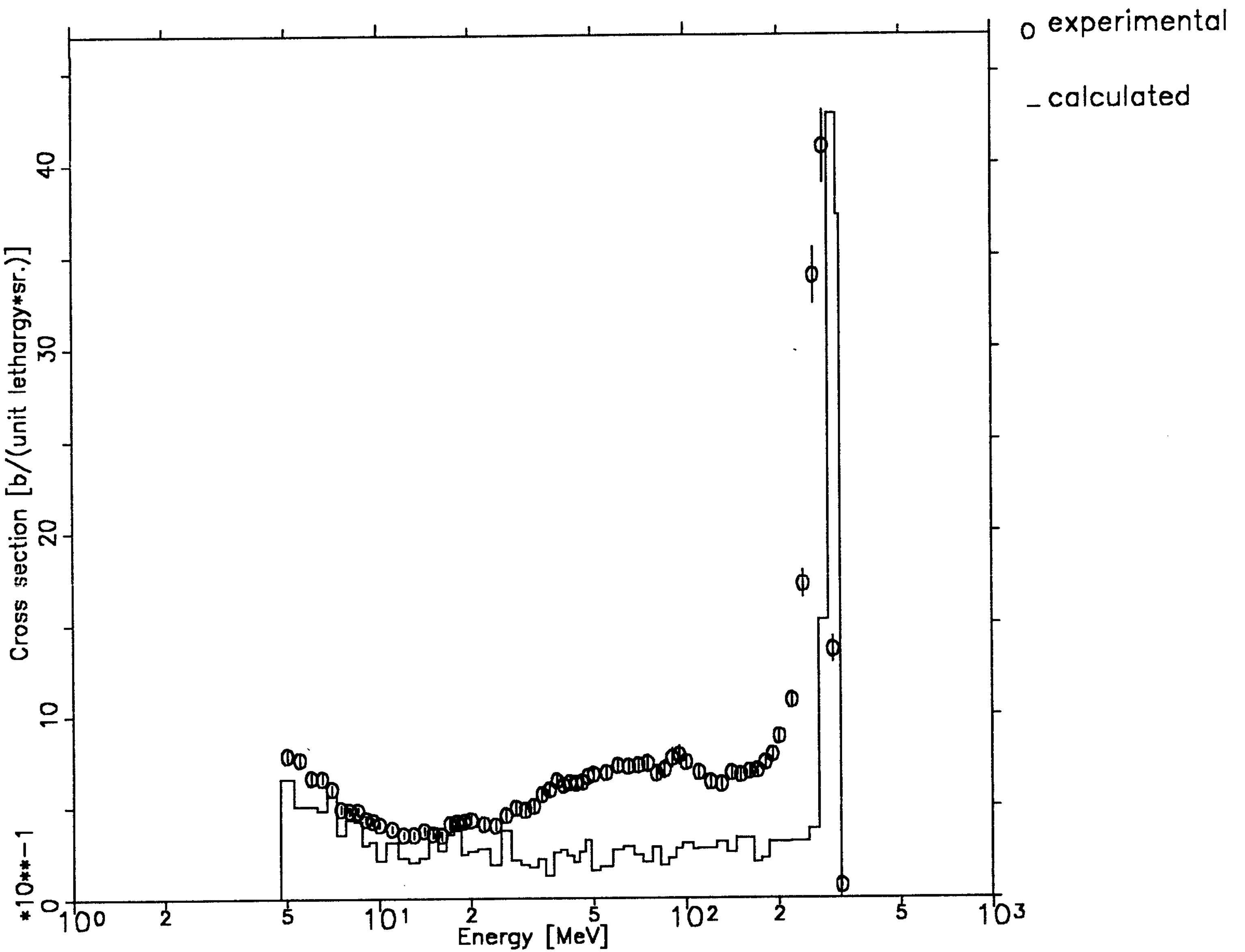

Fig. 11: cross section for neutron emission at 7.5 deg from Pb bombarded with 318 MeV protons:
Comparision of ToF–measurements and HETC–calculations

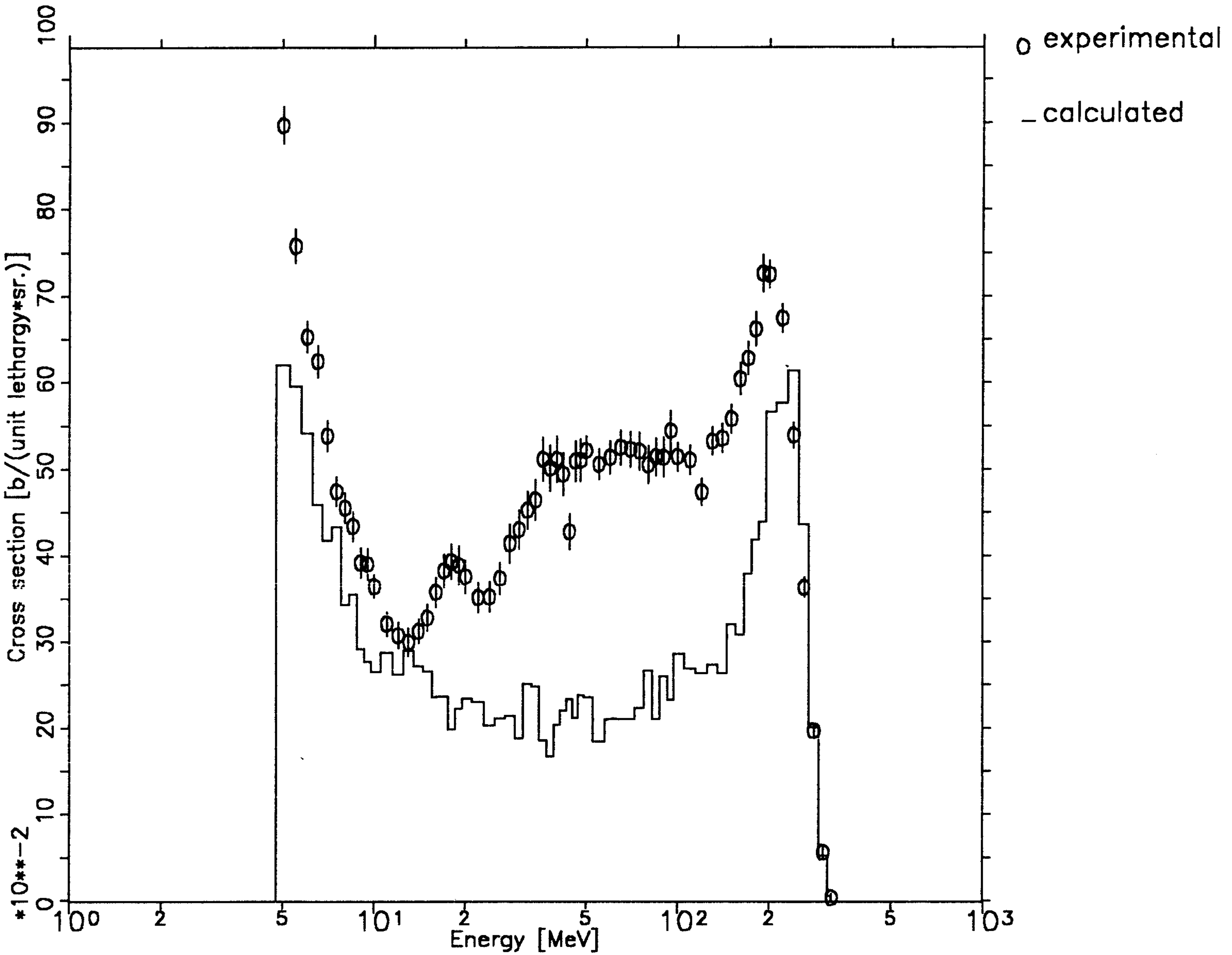

Fig. 12: Cross section for neutron emission at 30. deg from Pb bombarded with 318 MeV protons:
Comparision of ToF–measurements and HETC–calculations

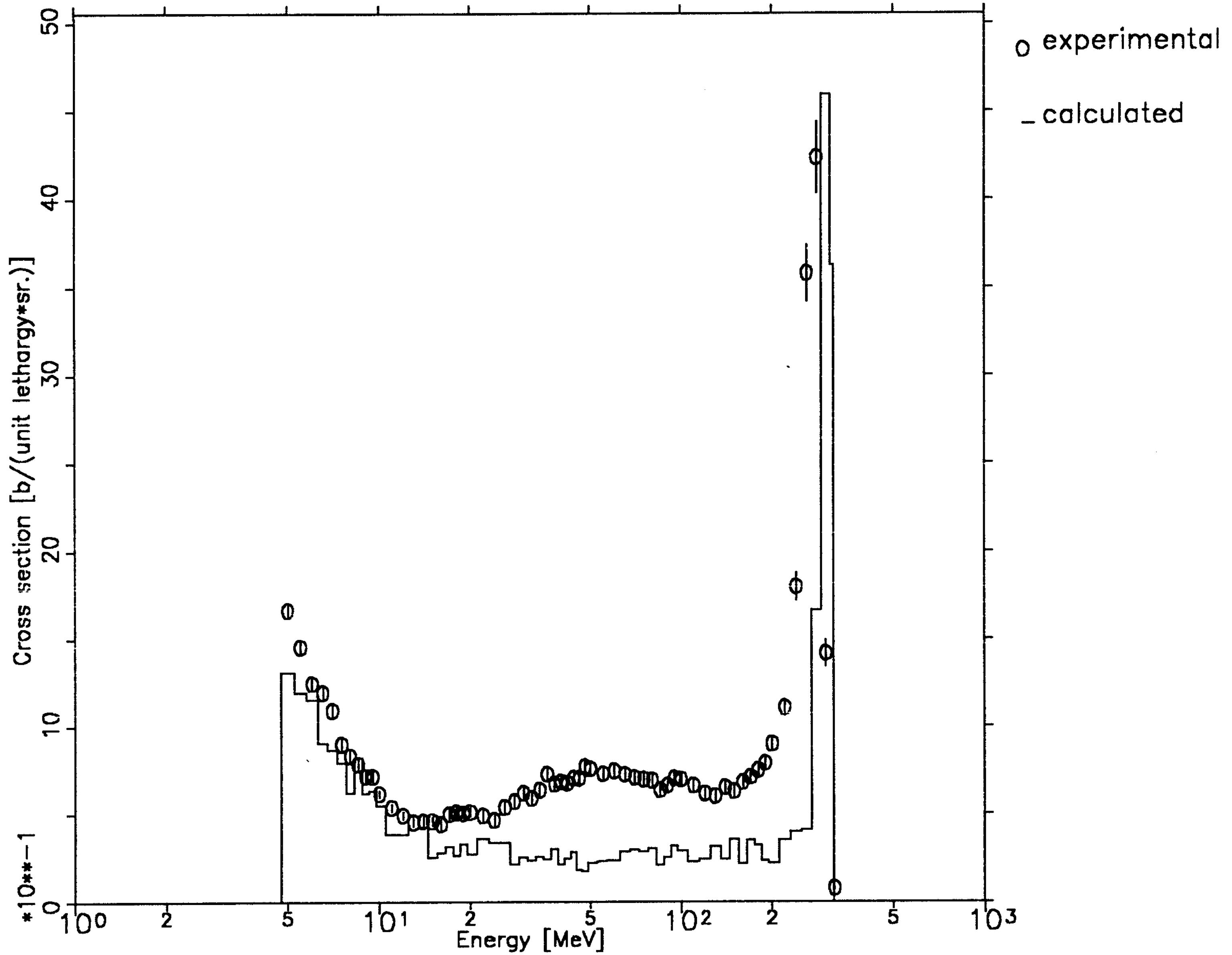

Fig. 13: cross section for neutron emission at 7.5 deg from U bombarded with 318 MeV protons:
Comparision of ToF–measurements and HETC–calculations

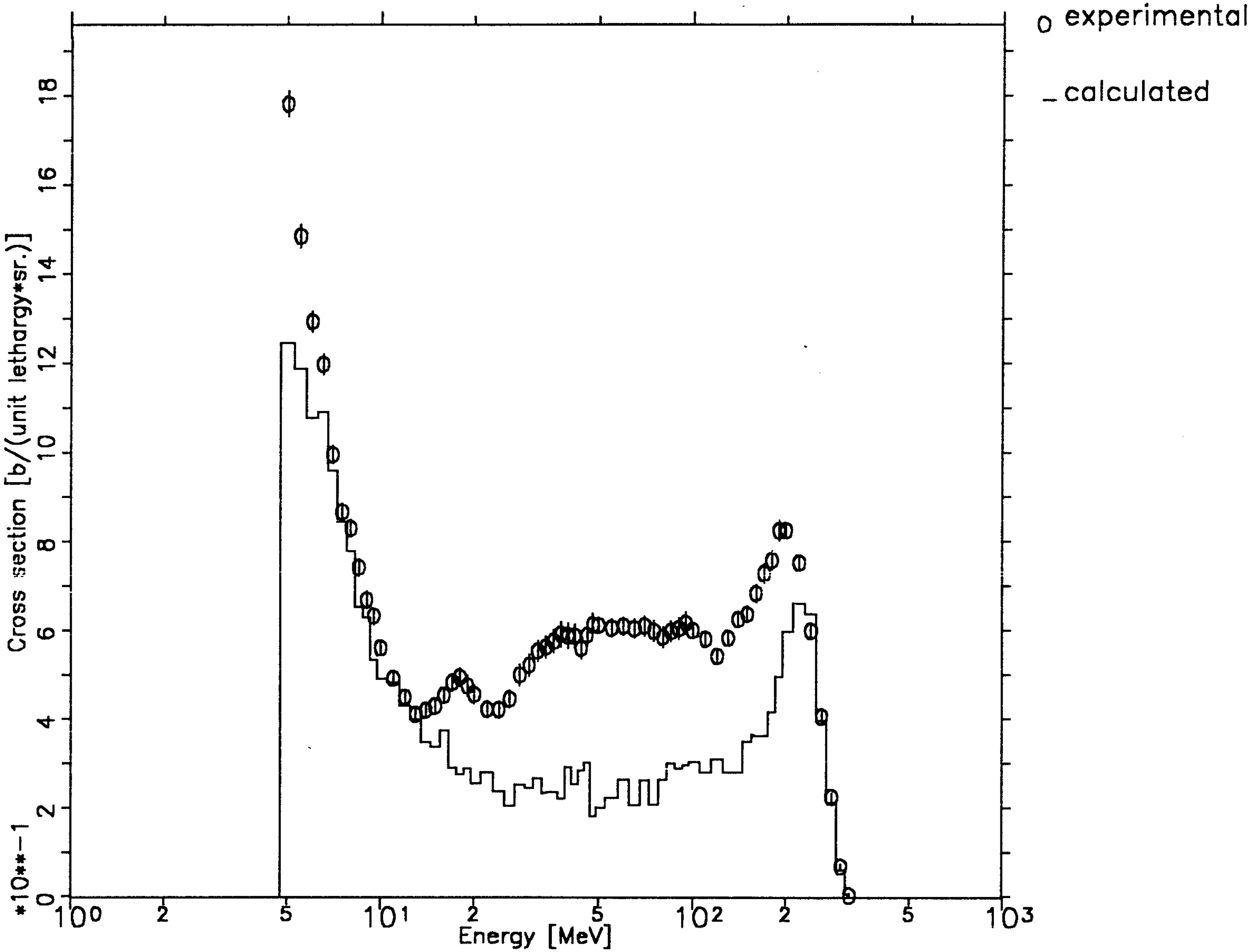

Fig. 14: Cross section for neutron emission at 30. deg from U bombarded with 318 MeV protons:
Comparision of ToF–measurements and HETC–calculations

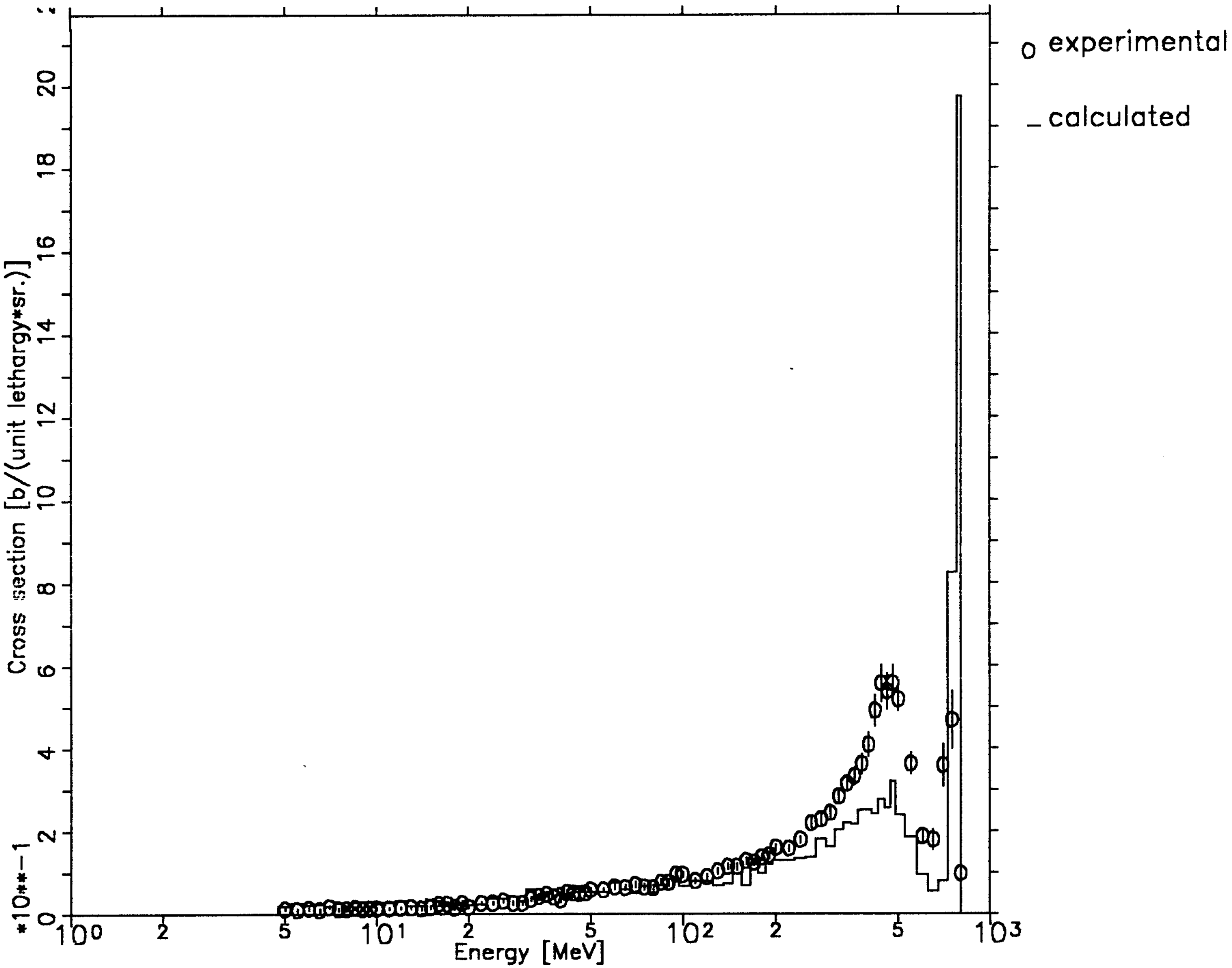

Fig. 15: cross section for neutron emission at 7.5 deg from C bombarded with 800 MeV protons:
Comparision of ToF–measurements and HETC–calculations

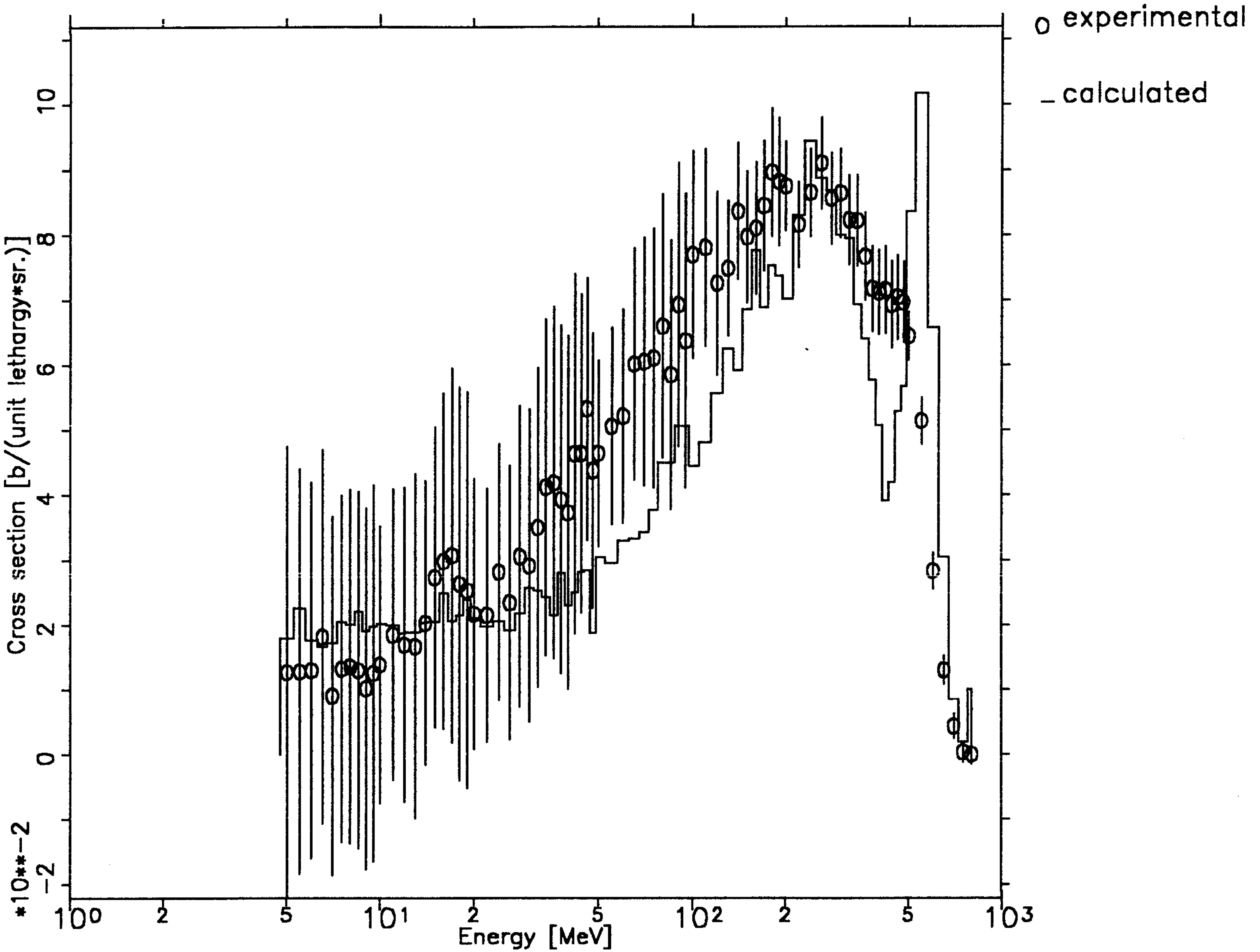

Fig. 16: Cross section for neutron emission at 30. deg from C bombarded with 800 MeV protons:
Comparision of ToF-measurements and HETC-calculations

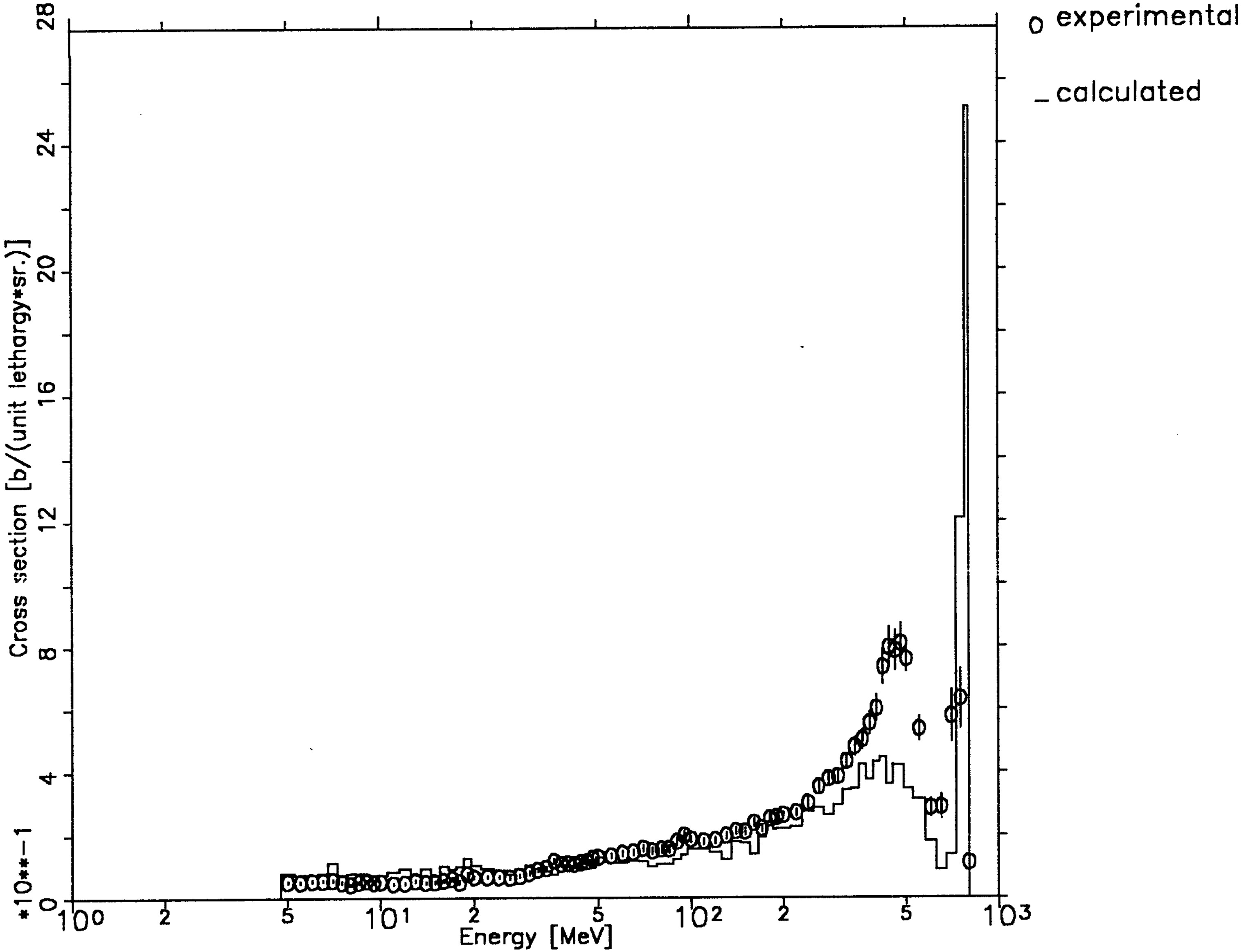

Fig. 17: cross section for neutron emission at 7.5 deg from Al bombarded with 800 MeV protons:
Comparision of ToF—measurements and HETC—calculations

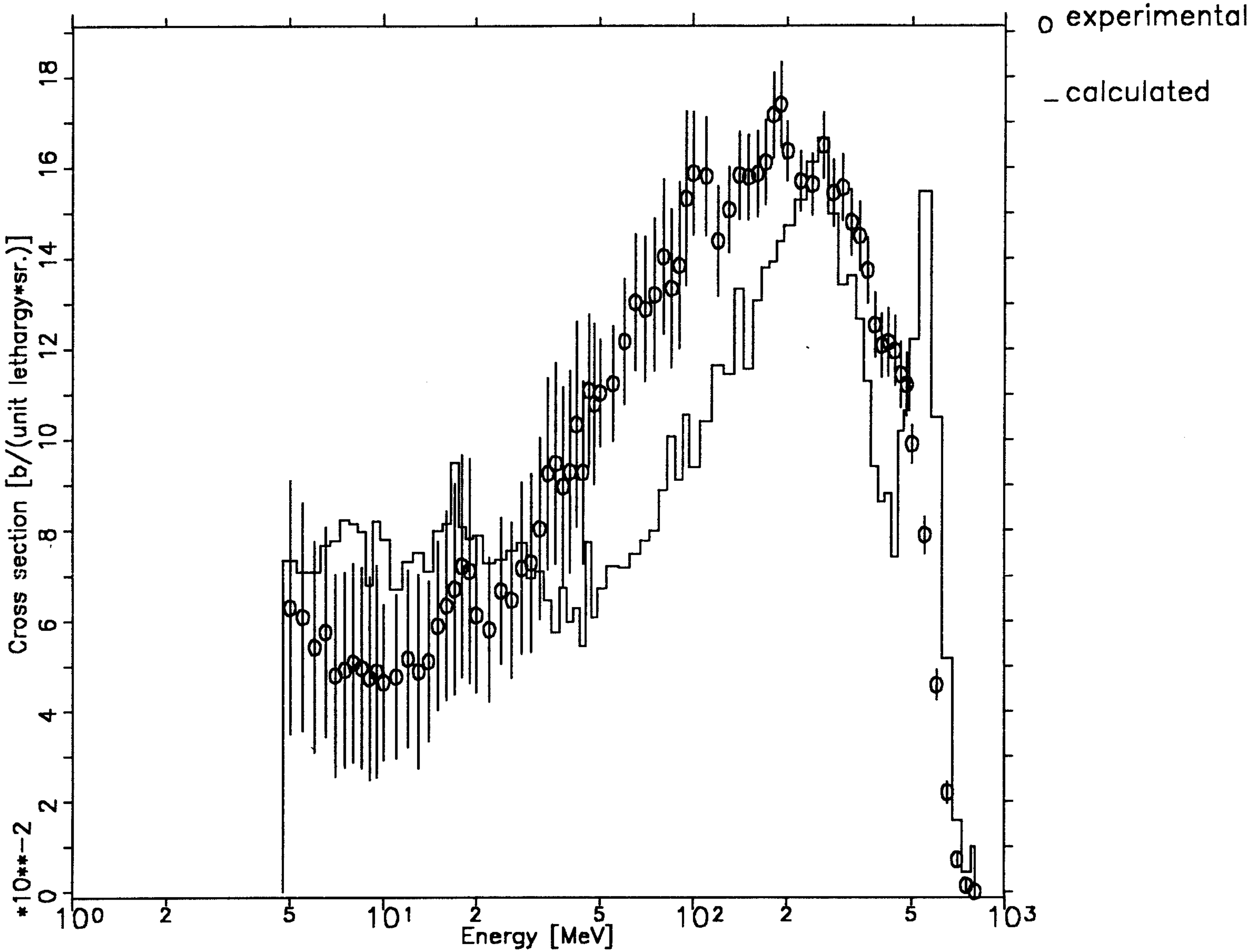

Fig. 18: Cross section for neutron emission at 30. deg from Al bombarded with 800 MeV protons:
Comparision of ToF-measurements and HETC-calculations

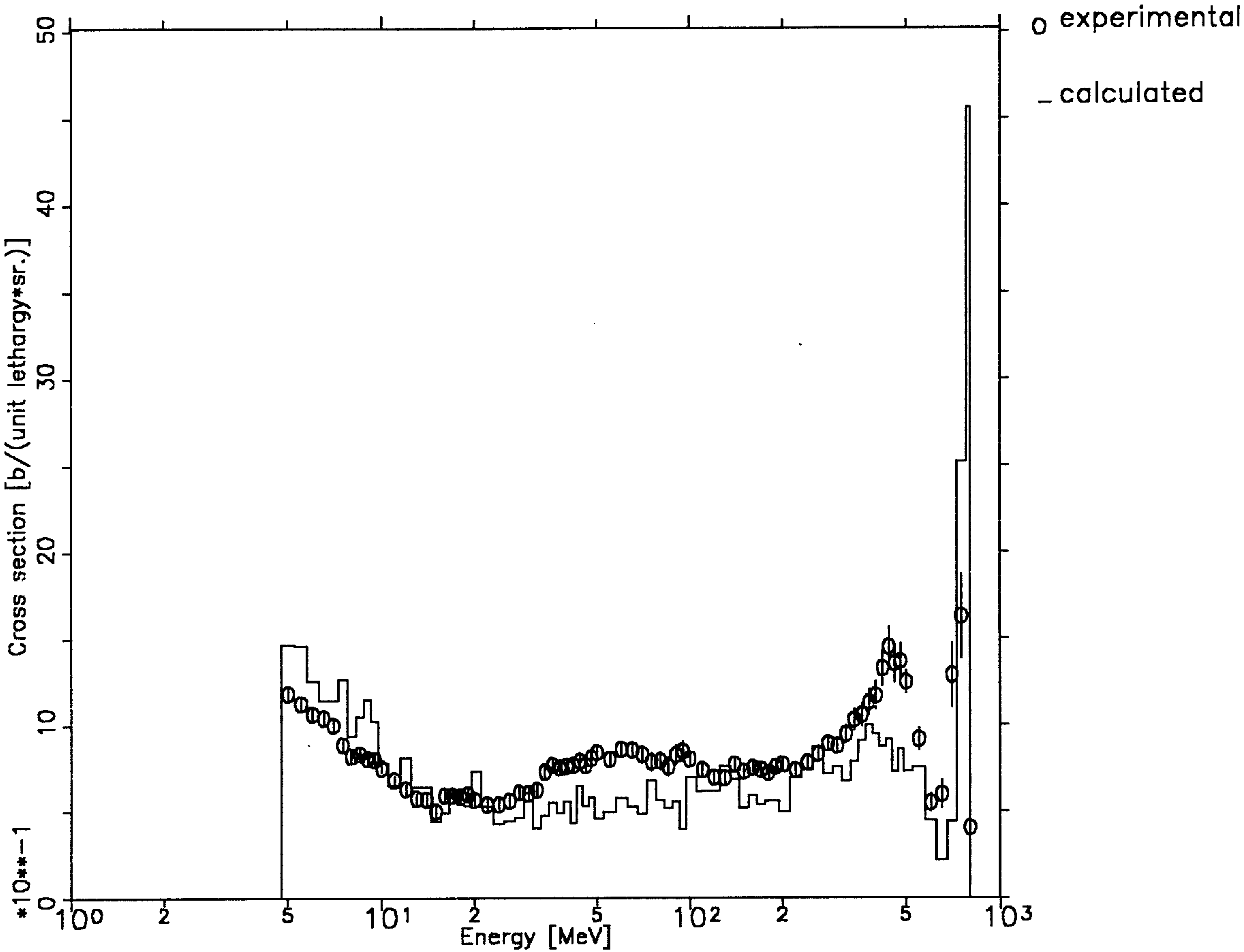

Fig. 19: cross section for neutron emission at 7.5 deg from Pb bombarded with 800 MeV protons:
Comparision of ToF–measurements and HETC–calculations

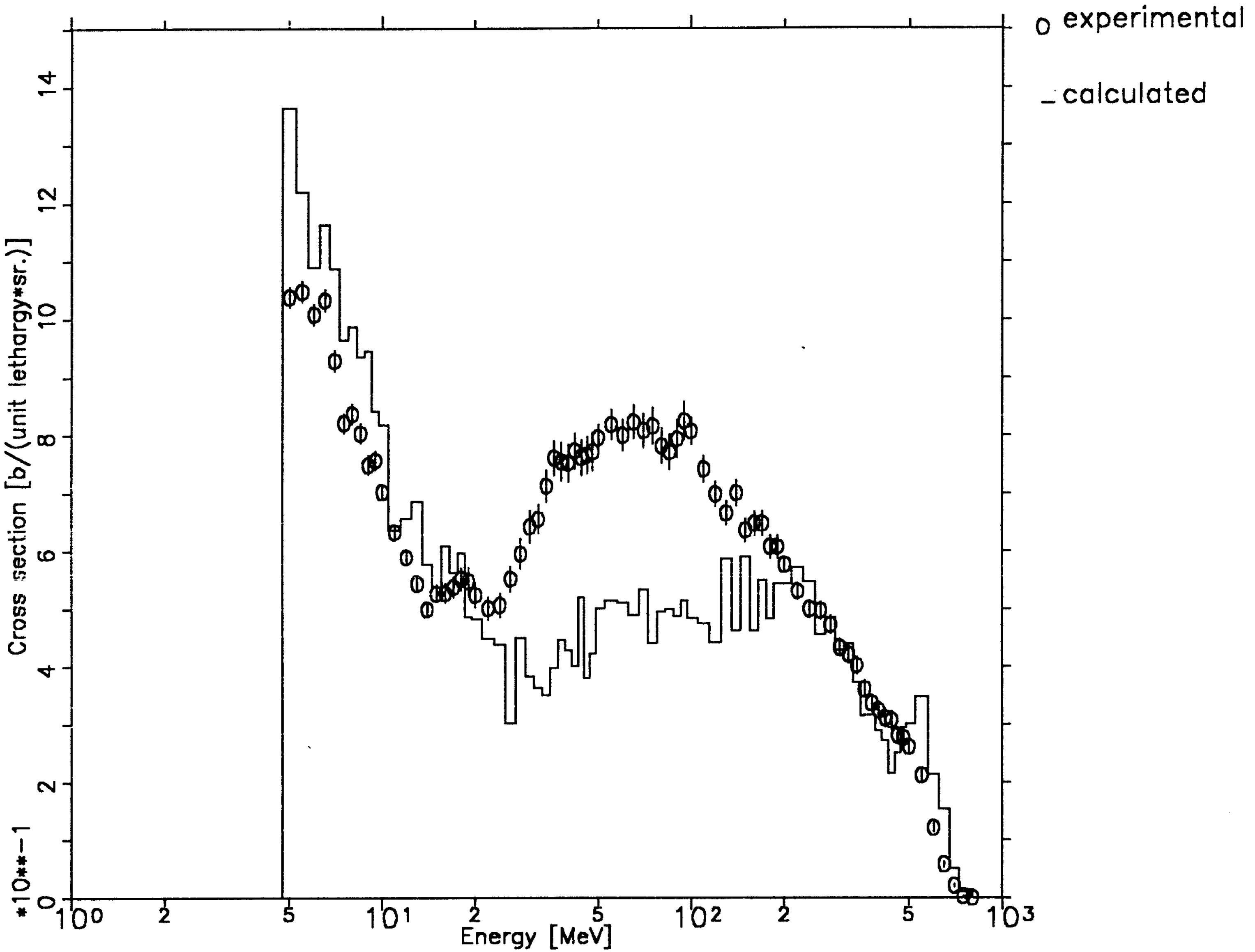

Fig. 20: Cross section for neutron emission at 30. deg from Pb bombarded with 800 MeV protons:
Comparision of ToF–measurements and HETC–calculations

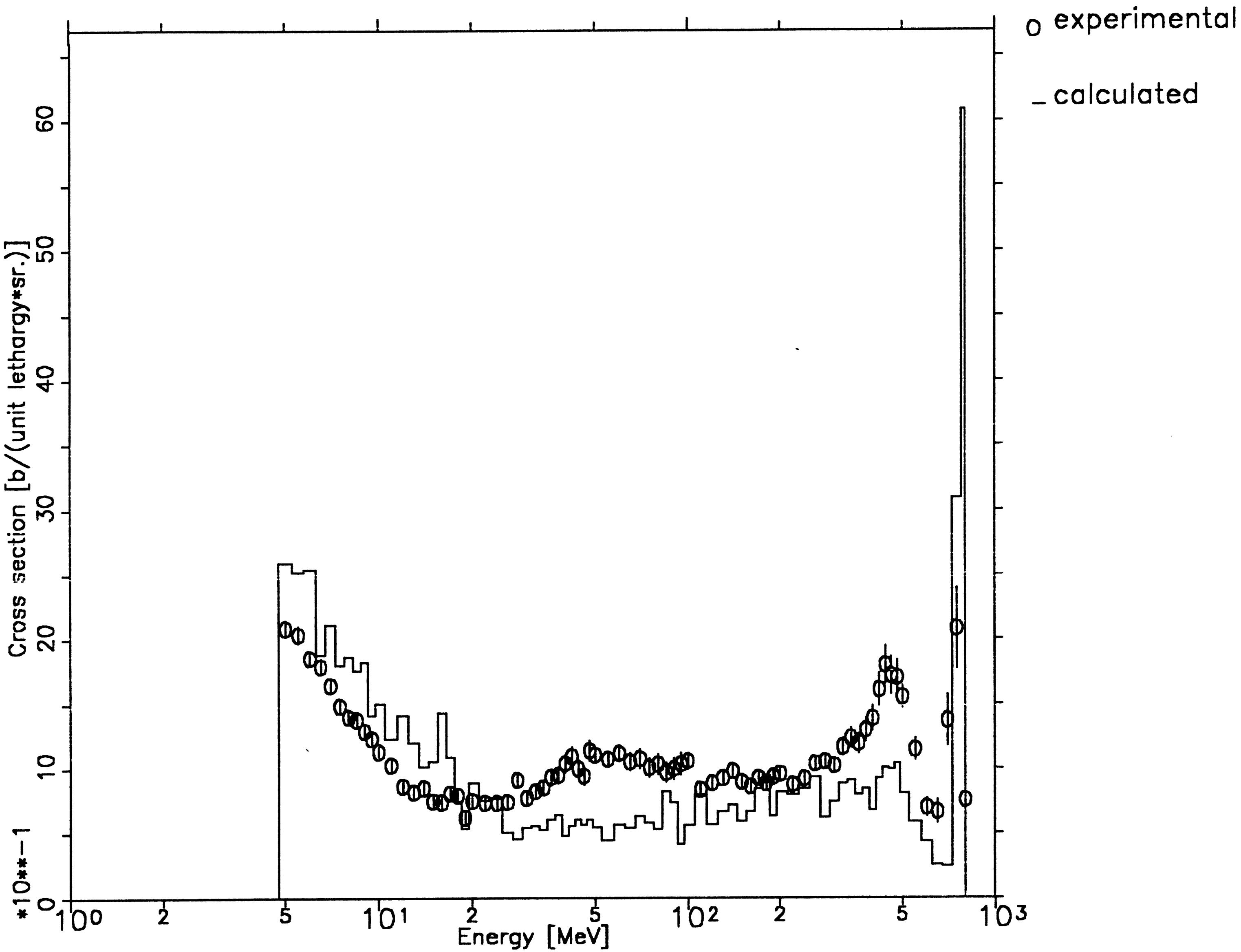

Fig. 21: cross section for neutron emission at 7.5 deg from U bombarded with 800 MeV protons:
Comparision of ToF—measurements and HETC—calculations

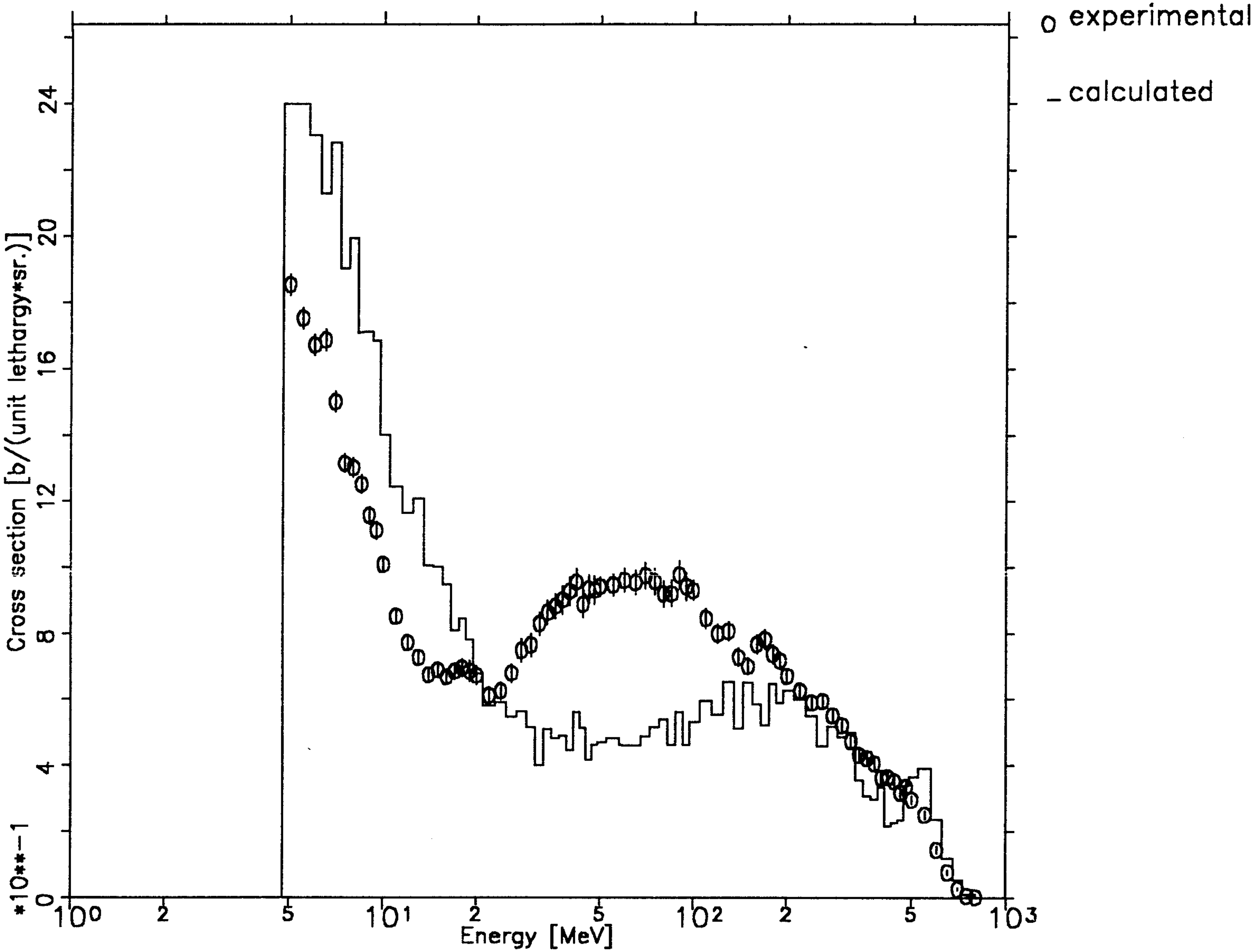

Fig. 22: Cross section for neutron emission at 30. deg from U bombarded with 800 MeV protons:
Comparision of ToF–measurements and HETC–calculations

Appendix C

The results of HETC/KFA-2 calculations of double differential cross sections of neutron emission into the angle intervals from 6-9 degrees and 28.5-31.5 degrees, respectively, are given in tables C-1 to C-6. The calculated cross sections are listed in units of barn/(MeV*steradian). Their total uncertainty FSD (one standard deviation) is given in percent.

List of tables:

Incident Energy : 318.MeV

Angle-interval : 6. - 9. degree

Target Elements:	C		Al		Ni		Ta	
Energy-Bin [MeV]	Cross-section [b/MeV/sr]	FSD [%]	Cross-section [b/MeV/sr]	FSD [%]	Cross-section [b/MeV/sr]	FSD [%]	Cross-section [b/MeV/sr]	FSD [%]
318. - 310.	0.211E-02	5.1	0.278E-02	4.2	0.314E-02	4.4	0.451E-02	6.0
310. - 290.	0.192E-02	2.7	0.276E-02	2.8	0.380E-02	3.2	0.615E-02	3.5
290. - 270.	0.164E-03	10.5	0.465E-03	7.3	0.738E-03	6.2	0.203E-02	5.7
270. - 250.	0.902E-04	13.2	0.156E-03	13.0	0.236E-03	10.9	0.664E-03	9.1
250. - 230.	0.776E-04	15.9	0.122E-03	14.6	0.250E-03	11.2	0.704E-03	10.6
230. - 210.	0.649E-04	14.5	0.158E-03	11.8	0.290E-03	10.0	0.483E-03	10.4
210. - 195.	0.697E-04	19.8	0.109E-03	16.3	0.282E-03	10.9	0.680E-03	10.1
195. - 185.	0.758E-04	23.7	0.163E-03	16.3	0.250E-03	15.2	0.550E-03	15.1
185. - 175.	0.830E-04	19.4	0.120E-03	20.0	0.282E-03	14.6	0.778E-03	13.0
175. - 165.	0.902E-04	20.8	0.101E-03	19.5	0.277E-03	12.7	0.738E-03	13.6
165. - 155.	0.685E-04	20.8	0.196E-03	15.5	0.217E-03	15.2	0.845E-03	12.3
155. - 145.	0.649E-04	21.4	0.225E-03	12.6	0.271E-03	13.8	0.644E-03	13.1
145. - 135.	0.649E-04	22.9	0.163E-03	15.2	0.304E-03	13.2	0.671E-03	12.5
135. - 125.	0.794E-04	18.9	0.134E-03	17.6	0.353E-03	13.6	0.711E-03	14.9
125. - 115.	0.685E-04	25.6	0.168E-03	15.9	0.358E-03	12.5	0.550E-03	18.4
115. - 105.	0.830E-04	22.2	0.177E-03	17.5	0.407E-03	11.1	0.845E-03	13.9
105. - 97.5	0.106E-03	21.0	0.172E-03	19.6	0.384E-03	13.9	0.106E-02	14.0
97.5 - 92.5	0.649E-04	32.0	0.220E-03	19.4	0.445E-03	16.4	0.121E-02	15.1
92.5 - 87.5	0.577E-04	34.1	0.230E-03	20.6	0.402E-03	16.2	0.993E-03	15.8
87.5 - 82.5	0.144E-03	22.5	0.268E-03	18.4	0.499E-03	14.5	0.126E-02	12.4
82.5 - 77.5	0.101E-03	24.9	0.230E-03	22.3	0.467E-03	17.1	0.118E-02	12.9
77.5 - 72.5	0.115E-03	24.7	0.306E-03	17.7	0.478E-03	14.8	0.110E-02	14.3
72.5 - 67.5	0.577E-04	34.1	0.297E-03	17.6	0.673E-03	14.1	0.966E-03	15.3
67.5 - 62.5	0.938E-04	26.0	0.316E-03	16.1	0.510E-03	13.6	0.137E-02	13.7
62.5 - 57.5	0.866E-04	29.7	0.287E-03	18.6	0.640E-03	14.6	0.140E-02	14.3
57.5 - 52.5	0.130E-03	21.4	0.249E-03	19.4	0.619E-03	13.4	0.166E-02	11.7
52.5 - 49.	0.165E-03	27.7	0.356E-03	19.4	0.589E-03	14.0	0.134E-02	19.4
49. - 47.	0.721E-04	49.2	0.359E-03	23.9	0.896E-03	17.2	0.134E-02	19.5
47. - 45.	0.144E-03	38.4	0.383E-03	26.2	0.706E-03	20.6	0.161E-02	21.7
45. - 43.	0.162E-03	32.0	0.407E-03	25.2	0.461E-03	24.1	0.188E-02	20.4
43. - 41.	0.144E-03	38.4	0.168E-03	36.6	0.896E-03	16.6	0.114E-02	21.7
41. - 39.	0.721E-04	49.2	0.263E-03	28.6	0.651E-03	19.3	0.201E-02	19.8
39. - 37.	0.180E-03	30.1	0.287E-03	29.7	0.923E-03	17.8	0.262E-02	13.6
37. - 35.	0.108E-03	39.8	0.335E-03	24.9	0.841E-03	19.2	0.215E-02	17.6
35. - 33.	0.162E-03	32.0	0.359E-03	25.7	0.706E-03	19.1	0.195E-02	17.9
33. - 31.	0.144E-03	34.1	0.455E-03	24.5	0.896E-03	18.2	0.255E-02	15.4
31. - 29.	0.162E-03	32.0	0.311E-03	26.0	0.950E-03	17.9	0.228E-02	20.4
29. - 27.	0.234E-03	26.0	0.335E-03	28.8	0.100E-02	19.5	0.342E-02	14.6
27. - 25.	0.253E-03	30.5	0.599E-03	20.0	0.114E-02	14.2	0.349E-02	14.5
25. - 23.	0.271E-03	29.0	0.479E-03	23.6	0.119E-02	16.8	0.409E-02	12.4
23. - 21.	0.343E-03	24.5	0.503E-03	24.7	0.163E-02	12.1	0.530E-02	11.2
21. - 19.5	0.289E-03	32.0	0.894E-03	22.2	0.127E-02	15.4	0.394E-02	15.5
19.5 - 18.5	0.108E-03	57.1	0.623E-03	28.2	0.136E-02	21.9	0.751E-02	14.2
18.5 - 17.5	0.325E-03	35.6	0.101E-02	25.6	0.114E-02	23.1	0.563E-02	15.9
17.5 - 16.5	0.253E-03	41.9	0.479E-03	33.3	0.195E-02	18.8	0.631E-02	17.1
16.5 - 15.5	0.253E-03	41.9	0.575E-03	32.0	0.141E-02	19.8	0.537E-02	16.7
15.5 - 14.5	0.289E-03	38.4	0.862E-03	25.4	0.244E-02	15.2	0.617E-02	15.7
14.5 - 13.5	0.505E-03	28.8	0.623E-03	28.2	0.201E-02	15.7	0.671E-02	14.1
13.5 - 12.5	0.361E-03	30.1	0.814E-03	22.2	0.277E-02	14.9	0.805E-02	12.7
12.5 - 11.5	0.469E-03	28.2	0.110E-02	19.4	0.353E-02	14.0	0.123E-01	9.8
11.5 - 10.5	0.433E-03	27.2	0.144E-02	19.2	0.369E-02	12.3	0.145E-01	10.0
10.5 - 9.75	0.481E-03	30.1	0.153E-02	23.0	0.376E-02	14.1	0.184E-01	9.2

Tab. C-1 : HETC/KFA-2 calculations of double differential cross sections for neutron emission at angles between 6. and 9. degree from targets elements C, Al, Ni and Ta induced by 318 MeV protons

Incident Energy : 318.MeV

Angle-interval : 6. - 9. degree

Target Elements:	C		Al		Ni		Ta	
Energy-Bin [MeV]	Cross-section [b/MeV/sr]	FSD [%]	Cross-section [b/MeV/sr]	FSD [%]	Cross-section [b/MeV/sr]	FSD [%]	Cross-section [b/MeV/sr]	FSD [%]
9.75 - 9.25	0.361E-03	43.8	0.105E-02	28.6	0.412E-02	16.7	0.239E-01	11.4
9.25 - 8.75	0.649E-03	35.6	0.125E-02	26.0	0.358E-02	20.6	0.241E-01	10.6
8.75 - 8.25	0.577E-03	34.1	0.201E-02	21.7	0.575E-02	14.6	0.231E-01	10.9
8.25 - 7.75	0.866E-03	29.7	0.192E-02	22.5	0.532E-02	12.8	0.295E-01	8.5
7.75 - 7.25	0.505E-03	36.6	0.287E-02	18.6	0.488E-02	14.1	0.279E-01	7.8
7.25 - 6.75	0.433E-03	39.8	0.211E-02	20.0	0.597E-02	13.4	0.338E-01	9.2
6.75 - 6.25	0.577E-03	34.1	0.230E-02	18.8	0.716E-02	11.6	0.357E-01	8.1
6.25 - 5.75	0.101E-02	24.9	0.278E-02	18.5	0.803E-02	11.7	0.478E-01	6.6
5.75 - 5.25	0.577E-03	38.4	0.220E-02	19.4	0.728E-02	12.5	0.582E-01	6.1
5.25 - 4.75	0.108E-02	25.7	0.201E-02	20.6	0.825E-02	13.7	0.606E-01	6.2

Tab. C-1 (cont.) : HETC/KFA-2 calculations of double differential cross sections for neutron emission at angles between 6. and 9. degree from targets elements C, Al, Ni and Ta induced by 318 MeV protons

Incident Energy : 318.MeV

Angle-interval : 28.5 - 31.5 degree

Target Elements:	C		Al		Ni		Ta	
Energy-Bin [MeV]	Cross-section [b/MeV/sr]	FSD [%]	Cross-section [b/MeV/sr]	FSD [%]	Cross-section [b/MeV/sr]	FSD [%]	Cross-section [b/MeV/sr]	FSD [%]
318. - 310.	0.353E-05	57.1	0.313E-05	70.4	0.531E-05	57.3	0.482E-04	28.2
310. - 290.	0.155E-04	16.7	0.506E-04	10.8	0.715E-04	9.6	0.117E-03	12.1
290. - 270.	0.673E-04	9.1	0.129E-03	6.9	0.208E-03	5.9	0.259E-03	8.2
270. - 250.	0.167E-03	5.5	0.284E-03	4.9	0.399E-03	4.1	0.728E-03	4.8
250. - 230.	0.257E-03	4.1	0.411E-03	4.2	0.574E-03	4.0	0.984E-03	2.9
230. - 210.	0.267E-03	3.9	0.447E-03	3.7	0.652E-03	3.3	0.116E-02	4.4
210. - 195.	0.232E-03	4.9	0.387E-03	4.3	0.580E-03	3.7	0.107E-02	4.4
195. - 185.	0.168E-03	7.7	0.358E-03	6.3	0.485E-03	5.1	0.104E-02	5.4
185. - 175.	0.147E-03	8.1	0.244E-03	6.5	0.436E-03	5.6	0.101E-02	5.6
175. - 165.	0.108E-03	9.1	0.243E-03	7.0	0.418E-03	5.8	0.928E-03	7.0
165. - 155.	0.961E-04	10.7	0.206E-03	8.5	0.385E-03	5.9	0.925E-03	7.1
155. - 145.	0.101E-03	9.2	0.208E-03	7.5	0.448E-03	5.4	0.774E-03	6.8
145. - 135.	0.904E-04	10.6	0.216E-03	8.3	0.370E-03	6.8	0.788E-03	6.3
135. - 125.	0.706E-04	12.2	0.199E-03	7.2	0.366E-03	7.4	0.728E-03	6.3
125. - 115.	0.744E-04	9.7	0.169E-03	6.9	0.364E-03	6.4	0.816E-03	6.0
115. - 105.	0.706E-04	10.9	0.176E-03	8.4	0.373E-03	6.6	0.946E-03	6.5
105. - 97.5	0.716E-04	12.8	0.190E-03	9.3	0.340E-03	8.2	0.841E-03	7.9
97.5 - 92.5	0.659E-04	17.4	0.175E-03	11.2	0.428E-03	8.1	0.113E-02	8.2
92.5 - 87.5	0.716E-04	17.1	0.253E-03	9.7	0.385E-03	8.8	0.981E-03	8.1
87.5 - 82.5	0.848E-04	15.6	0.233E-03	9.9	0.385E-03	7.6	0.114E-02	7.1
82.5 - 77.5	0.565E-04	18.0	0.178E-03	12.7	0.411E-03	7.4	0.112E-02	7.6
77.5 - 72.5	0.904E-04	14.9	0.220E-03	12.9	0.451E-03	7.7	0.115E-02	7.3
72.5 - 67.5	0.772E-04	16.7	0.260E-03	10.8	0.473E-03	7.3	0.117E-02	6.9
67.5 - 62.5	0.735E-04	14.1	0.253E-03	10.2	0.516E-03	7.0	0.124E-02	8.0
62.5 - 57.5	0.735E-04	15.8	0.240E-03	11.2	0.485E-03	7.5	0.154E-02	6.6
57.5 - 52.5	0.961E-04	12.0	0.255E-03	9.4	0.499E-03	8.0	0.144E-02	5.9
52.5 - 49.	0.118E-03	15.3	0.261E-03	10.5	0.672E-03	8.0	0.128E-02	8.7
49. - 47.	0.989E-04	22.8	0.238E-03	15.3	0.560E-03	10.7	0.182E-02	10.0
47. - 45.	0.989E-04	20.6	0.313E-03	11.2	0.673E-03	9.8	0.187E-02	10.0
45. - 43.	0.118E-03	20.0	0.313E-03	14.1	0.737E-03	8.8	0.117E-02	13.5
43. - 41.	0.989E-04	20.6	0.325E-03	13.2	0.659E-03	9.7	0.203E-02	10.4
41. - 39.	0.108E-03	23.8	0.400E-03	11.4	0.715E-03	8.9	0.194E-02	10.0
39. - 37.	0.179E-03	17.1	0.331E-03	14.6	0.758E-03	9.6	0.207E-02	9.1
37. - 35.	0.137E-03	17.9	0.294E-03	14.9	0.616E-03	12.0	0.252E-02	9.3
35. - 33.	0.151E-03	16.6	0.325E-03	14.1	0.815E-03	8.9	0.252E-02	7.9
33. - 31.	0.151E-03	15.9	0.369E-03	12.3	0.928E-03	7.8	0.243E-02	9.0
31. - 29.	0.141E-03	19.2	0.331E-03	13.3	0.850E-03	8.4	0.229E-02	9.9
29. - 27.	0.170E-03	16.5	0.463E-03	11.6	0.101E-02	8.5	0.284E-02	8.3
27. - 25.	0.137E-03	19.8	0.400E-03	12.3	0.101E-02	8.4	0.350E-02	6.8
25. - 23.	0.193E-03	15.1	0.563E-03	11.6	0.103E-02	7.7	0.371E-02	7.0
23. - 21.	0.198E-03	15.6	0.650E-03	10.3	0.122E-02	8.2	0.468E-02	7.1
21. - 19.5	0.195E-03	20.4	0.525E-03	13.1	0.141E-02	10.2	0.427E-02	7.1
19.5 - 18.5	0.245E-03	22.3	0.838E-03	12.4	0.149E-02	11.1	0.546E-02	8.1
18.5 - 17.5	0.254E-03	21.0	0.713E-03	13.3	0.177E-02	10.7	0.539E-02	8.1
17.5 - 16.5	0.367E-03	18.6	0.850E-03	11.8	0.157E-02	10.3	0.658E-02	6.5
16.5 - 15.5	0.311E-03	18.3	0.950E-03	13.9	0.180E-02	9.4	0.732E-02	7.8
15.5 - 14.5	0.188E-03	22.5	0.813E-03	11.4	0.194E-02	9.8	0.711E-02	7.7
14.5 - 13.5	0.264E-03	19.7	0.101E-02	10.6	0.183E-02	9.9	0.858E-02	7.0
13.5 - 12.5	0.339E-03	18.3	0.713E-03	11.8	0.221E-02	8.5	0.865E-02	6.8
12.5 - 11.5	0.330E-03	17.4	0.863E-03	10.6	0.292E-02	6.8	0.117E-01	4.9
11.5 - 10.5	0.339E-03	16.1	0.129E-02	10.9	0.289E-02	7.1	0.130E-01	4.6
10.5 - 9.75	0.502E-03	15.9	0.132E-02	10.2	0.357E-02	7.3	0.159E-01	4.6

Tab. C-2 : HETC/KFA-2 calculations of double differential cross sections for neutron emission at angles between 28.5 and 31.5 degree from targets elements C, Al, Ni and Ta induced by 318 MeV protons

Incident Energy : 318.MeV

Angle-interval : 28.5 - 31.5 degree

Target Elements:	C		Al		Ni		Ta	
Energy-Bin [MeV]	Cross-section [b/MeV/sr]	FSD [%]	Cross-section [b/MeV/sr]	FSD [%]	Cross-section [b/MeV/sr]	FSD [%]	Cross-section [b/MeV/sr]	FSD [%]
9.75 - 9.25	0.527E-03	18.4	0.145E-02	13.0	0.411E-02	8.3	0.206E-01	5.0
9.25 - 8.75	0.565E-03	16.8	0.143E-02	12.3	0.419E-02	8.6	0.181E-01	6.6
8.75 - 8.25	0.659E-03	15.4	0.115E-02	14.3	0.453E-02	9.6	0.226E-01	5.0
8.25 - 7.75	0.452E-03	20.6	0.120E-02	15.5	0.499E-02	7.5	0.247E-01	5.5
7.75 - 7.25	0.584E-03	17.6	0.208E-02	10.4	0.592E-02	6.8	0.288E-01	4.5
7.25 - 6.75	0.603E-03	17.7	0.208E-02	10.4	0.558E-02	8.4	0.333E-01	4.8
6.75 - 6.25	0.885E-03	15.9	0.205E-02	10.4	0.618E-02	6.9	0.325E-01	4.6
6.25 - 5.75	0.716E-03	16.6	0.233E-02	11.7	0.836E-02	5.3	0.417E-01	4.0
5.75 - 5.25	0.753E-03	16.3	0.283E-02	8.8	0.765E-02	6.3	0.526E-01	3.2
5.25 - 4.75	0.452E-03	22.3	0.308E-02	8.3	0.887E-02	5.5	0.649E-01	3.5

Tab. C-2 (cont.) : HETC/KFA-2 calculations of double differential cross sections for neutron emission at angles between 28.5 and 31.5 degree from targets elements C, Al, Ni and Ta induced by 318 MeV protons

Incident Energy : 318.MeV

Angle-interval : 6. - 9. degree

Target Elements: W Pb U

Energy-Bin [MeV]	W Cross-section [b/MeV/sr]	W FSD [%]	Pb Cross-section [b/MeV/sr]	Pb FSD [%]	U Cross-section [b/MeV/sr]	U FSD [%]
318. - 310.	0.481E-02	5.5	0.515E-02	7.1	0.502E-02	8.5
310. - 290.	0.616E-02	3.7	0.619E-02	4.0	0.665E-02	4.5
290. - 270.	0.238E-02	4.9	0.236E-02	6.7	0.258E-02	7.0
270. - 250.	0.547E-03	11.6	0.629E-03	13.6	0.685E-03	12.7
250. - 230.	0.500E-03	12.6	0.561E-03	12.5	0.722E-03	13.4
230. - 210.	0.561E-03	12.8	0.607E-03	12.8	0.697E-03	13.5
210. - 195.	0.514E-03	13.3	0.656E-03	15.9	0.473E-03	22.1
195. - 185.	0.446E-03	19.1	0.710E-03	15.9	0.538E-03	21.7
185. - 175.	0.716E-03	12.6	0.526E-03	17.8	0.783E-03	16.6
175. - 165.	0.324E-03	24.7	0.504E-03	19.6	0.905E-03	17.6
165. - 155.	0.689E-03	13.2	0.893E-03	14.8	0.587E-03	20.0
155. - 145.	0.622E-03	16.3	0.961E-03	15.0	0.103E-02	17.5
145. - 135.	0.635E-03	15.4	0.778E-03	18.5	0.758E-03	17.8
135. - 125.	0.851E-03	12.7	0.103E-02	16.6	0.105E-02	15.9
125. - 115.	0.797E-03	13.6	0.984E-03	14.9	0.881E-03	15.4
115. - 105.	0.111E-02	11.6	0.105E-02	14.2	0.905E-03	15.4
105. - 97.5	0.955E-03	13.1	0.128E-02	15.7	0.124E-02	18.6
97.5 - 92.5	0.946E-03	16.7	0.124E-02	21.3	0.147E-02	17.2
92.5 - 87.5	0.165E-02	13.0	0.105E-02	21.7	0.122E-02	18.3
87.5 - 82.5	0.151E-02	13.3	0.916E-03	23.7	0.108E-02	23.6
82.5 - 77.5	0.141E-02	12.3	0.151E-02	16.6	0.166E-02	17.6
77.5 - 72.5	0.157E-02	13.2	0.114E-02	21.6	0.166E-02	17.0
72.5 - 67.5	0.157E-02	11.5	0.146E-02	18.3	0.186E-02	15.3
67.5 - 62.5	0.165E-02	13.6	0.188E-02	17.0	0.191E-02	18.1
62.5 - 57.5	0.138E-02	12.9	0.192E-02	15.0	0.171E-02	16.4
57.5 - 52.5	0.154E-02	12.8	0.137E-02	21.3	0.181E-02	17.6
52.5 - 49.	0.205E-02	12.6	0.131E-02	21.4	0.189E-02	16.9
49. - 47.	0.142E-02	21.1	0.286E-02	20.0	0.159E-02	28.7
47. - 45.	0.196E-02	19.8	0.240E-02	22.6	0.171E-02	25.1
45. - 43.	0.304E-02	15.8	0.195E-02	24.7	0.281E-02	20.8
43. - 41.	0.182E-02	23.5	0.240E-02	21.6	0.257E-02	20.5
41. - 39.	0.230E-02	17.1	0.286E-02	18.3	0.232E-02	21.1
39. - 37.	0.297E-02	13.3	0.286E-02	20.8	0.342E-02	19.2
37. - 35.	0.351E-02	11.6	0.149E-02	26.5	0.294E-02	21.7
35. - 33.	0.318E-02	15.1	0.275E-02	23.2	0.330E-02	20.6
33. - 31.	0.378E-02	16.7	0.229E-02	18.9	0.318E-02	18.4
31. - 29.	0.297E-02	14.8	0.263E-02	20.8	0.367E-02	20.2
29. - 27.	0.378E-02	12.8	0.320E-02	22.3	0.330E-02	21.9
27. - 25.	0.358E-02	12.3	0.618E-02	13.4	0.563E-02	13.5
25. - 23.	0.385E-02	13.3	0.332E-02	18.5	0.612E-02	12.8
23. - 21.	0.446E-02	12.0	0.538E-02	19.1	0.709E-02	12.2
21. - 19.5	0.577E-02	11.9	0.549E-02	17.8	0.587E-02	15.9
19.5 - 18.5	0.554E-02	14.7	0.549E-02	23.2	0.758E-02	18.4
18.5 - 17.5	0.527E-02	17.1	0.938E-02	17.0	0.636E-02	20.0
17.5 - 16.5	0.662E-02	13.8	0.893E-02	19.1	0.807E-02	17.1
16.5 - 15.5	0.689E-02	15.4	0.710E-02	17.8	0.758E-02	15.9
15.5 - 14.5	0.730E-02	13.9	0.110E-01	13.6	0.734E-02	19.6
14.5 - 13.5	0.892E-02	14.3	0.687E-02	21.3	0.132E-01	11.5
13.5 - 12.5	0.919E-02	11.5	0.664E-02	17.1	0.164E-01	9.9
12.5 - 11.5	0.112E-01	10.2	0.801E-02	19.7	0.139E-01	15.4
11.5 - 10.5	0.143E-01	9.0	0.121E-01	12.2	0.154E-01	12.0
10.5 - 9.75	0.160E-01	11.0	0.885E-02	17.8	0.235E-01	9.9

Tab. C-3 : HETC/KFA-2 calculations of double differential cross sections for neutron emission at angles between 6. and 9. degree from targets elements W, Pb and U induced by 318 MeV protons

Incident Energy : 318.MeV

Angle-interval : 6. - 9. degree

Target Elements: W Pb U

Energy-Bin [MeV]	W Cross-section [b/MeV/sr]	W FSD [%]	Pb Cross-section [b/MeV/sr]	Pb FSD [%]	U Cross-section [b/MeV/sr]	U FSD [%]
9.75 - 9.25	0.230E-01	11.6	0.142E-01	17.8	0.289E-01	14.1
9.25 - 8.75	0.230E-01	10.8	0.142E-01	17.2	0.298E-01	15.6
8.75 - 8.25	0.278E-01	12.0	0.215E-01	15.0	0.421E-01	10.9
8.25 - 7.75	0.227E-01	10.4	0.233E-01	13.3	0.338E-01	12.1
7.75 - 7.25	0.387E-01	8.5	0.201E-01	15.4	0.460E-01	10.0
7.25 - 6.75	0.395E-01	8.1	0.348E-01	11.9	0.538E-01	9.2
6.75 - 6.25	0.335E-01	8.8	0.320E-01	11.0	0.607E-01	8.4
6.25 - 5.75	0.487E-01	6.6	0.366E-01	10.1	0.837E-01	6.8
5.75 - 5.25	0.689E-01	8.2	0.403E-01	10.3	0.944E-01	7.0
5.25 - 4.75	0.665E-01	7.3	0.568E-01	10.1	0.114E+00	5.7

Tab. C-3 (cont.) : HETC/KFA-2 calculations of double differential cross sections for neutron emission at angles between 6. and 9. degree from targets elements W, Pb and U induced by 318 MeV protons

Incident Energy : 318.MeV

Angle-interval : 28.5 - 31.5 degree

Target Elements: W Pb U

Energy-Bin [MeV]	W Cross-section [b/MeV/sr]	W FSD [%]	Pb Cross-section [b/MeV/sr]	Pb FSD [%]	U Cross-section [b/MeV/sr]	U FSD [%]
318. - 310.	0.132E-04	57.0	0.747E-05	100.0	0.798E-05	100.0
310. - 290.	0.864E-04	14.4	0.747E-04	20.0	0.862E-04	20.6
290. - 270.	0.275E-03	8.6	0.311E-03	10.4	0.329E-03	9.8
270. - 250.	0.669E-03	5.2	0.729E-03	6.7	0.661E-03	6.1
250. - 230.	0.887E-03	4.5	0.111E-02	4.0	0.115E-02	4.9
230. - 210.	0.126E-02	3.6	0.114E-02	4.6	0.130E-02	5.0
210. - 195.	0.108E-02	4.2	0.121E-02	5.4	0.128E-02	6.2
195. - 185.	0.946E-03	6.9	0.100E-02	7.6	0.113E-02	7.8
185. - 175.	0.861E-03	7.2	0.101E-02	6.6	0.100E-02	6.9
175. - 165.	0.106E-02	5.4	0.968E-03	6.6	0.926E-03	9.6
165. - 155.	0.914E-03	6.3	0.837E-03	7.9	0.990E-03	7.8
155. - 145.	0.674E-03	7.5	0.926E-03	8.5	0.101E-02	6.9
145. - 135.	0.868E-03	7.2	0.819E-03	9.3	0.869E-03	9.6
135. - 125.	0.808E-03	5.8	0.914E-03	8.0	0.932E-03	7.7
125. - 115.	0.931E-03	6.0	0.956E-03	8.8	0.112E-02	7.8
115. - 105.	0.882E-03	6.8	0.106E-02	7.3	0.110E-02	7.6
105. - 97.5	0.969E-03	7.5	0.123E-02	7.2	0.130E-02	7.7
97.5 - 92.5	0.967E-03	7.3	0.106E-02	10.7	0.135E-02	9.1
92.5 - 87.5	0.868E-03	11.0	0.125E-02	8.6	0.139E-02	10.5
87.5 - 82.5	0.100E-02	7.4	0.108E-02	9.5	0.153E-02	11.5
82.5 - 77.5	0.128E-02	6.4	0.145E-02	9.9	0.143E-02	10.2
77.5 - 72.5	0.133E-02	7.7	0.129E-02	10.0	0.120E-02	9.3
72.5 - 67.5	0.140E-02	9.2	0.130E-02	9.0	0.162E-02	8.0
67.5 - 62.5	0.119E-02	8.2	0.141E-02	8.3	0.138E-02	9.8
62.5 - 57.5	0.142E-02	8.4	0.152E-02	8.6	0.190E-02	7.5
57.5 - 52.5	0.162E-02	7.1	0.146E-02	8.9	0.175E-02	6.6
52.5 - 49.	0.165E-02	7.8	0.201E-02	8.7	0.172E-02	8.3
49. - 47.	0.178E-02	8.3	0.215E-02	9.8	0.163E-02	13.9
47. - 45.	0.175E-02	9.3	0.200E-02	11.4	0.284E-02	10.9
45. - 43.	0.185E-02	10.1	0.230E-02	12.2	0.281E-02	9.0
43. - 41.	0.127E-02	12.1	0.227E-02	11.9	0.262E-02	10.4
41. - 39.	0.215E-02	7.8	0.221E-02	10.4	0.316E-02	12.1
39. - 37.	0.224E-02	8.1	0.191E-02	15.1	0.252E-02	10.4
37. - 35.	0.235E-02	8.9	0.224E-02	12.2	0.284E-02	11.8
35. - 33.	0.251E-02	7.7	0.317E-02	8.9	0.297E-02	11.0
33. - 31.	0.191E-02	11.8	0.341E-02	8.8	0.361E-02	9.8
31. - 29.	0.298E-02	7.8	0.272E-02	8.0	0.354E-02	9.8
29. - 27.	0.332E-02	7.3	0.332E-02	8.4	0.390E-02	9.6
27. - 25.	0.337E-02	7.4	0.353E-02	8.0	0.342E-02	8.6
25. - 23.	0.404E-02	6.6	0.367E-02	8.3	0.428E-02	7.9
23. - 21.	0.362E-02	7.7	0.454E-02	8.1	0.552E-02	6.4
21. - 19.5	0.463E-02	6.4	0.502E-02	11.2	0.545E-02	8.3
19.5 - 18.5	0.547E-02	7.2	0.508E-02	11.7	0.658E-02	10.6
18.5 - 17.5	0.515E-02	9.0	0.478E-02	11.3	0.664E-02	10.5
17.5 - 16.5	0.519E-02	8.1	0.603E-02	8.4	0.741E-02	9.9
16.5 - 15.5	0.734E-02	7.6	0.639E-02	9.0	0.102E-01	9.4
15.5 - 14.5	0.847E-02	7.2	0.771E-02	11.2	0.977E-02	10.3
14.5 - 13.5	0.868E-02	5.9	0.843E-02	8.6	0.108E-01	7.6
13.5 - 12.5	0.893E-02	5.7	0.968E-02	9.0	0.133E-01	7.2
12.5 - 11.5	0.116E-01	5.9	0.950E-02	6.9	0.156E-01	7.0
11.5 - 10.5	0.134E-01	5.4	0.114E-01	7.3	0.190E-01	6.6
10.5 - 9.75	0.163E-01	5.6	0.114E-01	7.2	0.210E-01	6.7

Tab. C-4 : HETC/KFA-2 calculations of double differential cross sections for neutron emission at angles between 28.5 and 31.5 degree from targets elements W, Pb and U induced by 318 MeV protons

Incident Energy : 318.MeV

Angle-interval : 28.5 - 31.5 degree

Target Elements: W Pb U

Energy-Bin [MeV]	W Cross-section [b/MeV/sr]	W FSD [%]	Pb Cross-section [b/MeV/sr]	Pb FSD [%]	U Cross-section [b/MeV/sr]	U FSD [%]
9.75 - 9.25	0.180E-01	5.8	0.127E-01	10.2	0.244E-01	8.4
9.25 - 8.75	0.207E-01	5.5	0.141E-01	9.2	0.304E-01	6.1
8.75 - 8.25	0.223E-01	6.6	0.182E-01	7.5	0.333E-01	4.8
8.25 - 7.75	0.260E-01	5.4	0.186E-01	6.9	0.423E-01	4.6
7.75 - 7.25	0.329E-01	4.9	0.251E-01	7.0	0.489E-01	4.6
7.25 - 6.75	0.382E-01	4.0	0.259E-01	7.1	0.595E-01	4.2
6.75 - 6.25	0.365E-01	4.3	0.307E-01	6.5	0.729E-01	3.4
6.25 - 5.75	0.481E-01	3.3	0.392E-01	5.6	0.780E-01	4.3
5.75 - 5.25	0.531E-01	3.3	0.471E-01	5.0	0.939E-01	3.4
5.25 - 4.75	0.716E-01	3.1	0.539E-01	4.3	0.108E+00	3.6

Tab. C-4 (cont.) : HETC/KFA-2 calculations of double differential cross sections for neutron emission at angles between 28.5 and 31.5 degree from targets elements W, Pb and U induced by 318 MeV protons

Incident Energy : 800.MeV

Angle-interval : 6. - 9. degree

Target Elements:	C		Al		Pb		U	
Energy-Bin [MeV]	Cross-section [b/MeV/sr]	FSD [%]	Cross-section [b/MeV/sr]	FSD [%]	Cross-section [b/MeV/sr]	FSD [%]	Cross-section [b/MeV/sr]	FSD [%]
800. - 775.	0.109E-02	3.6	0.139E-02	3.7	0.252E-02	5.2	0.336E-02	4.6
775. - 725.	0.478E-03	4.1	0.699E-03	3.3	0.146E-02	5.0	0.179E-02	5.4
725. - 675.	0.491E-04	12.2	0.852E-04	11.8	0.275E-03	12.8	0.152E-03	11.2
675. - 625.	0.368E-04	12.0	0.594E-04	11.9	0.146E-03	19.3	0.171E-03	14.3
625. - 575.	0.693E-04	11.6	0.131E-03	8.0	0.325E-03	10.7	0.318E-03	14.8
575. - 525.	0.146E-03	6.2	0.248E-03	6.5	0.595E-03	9.4	0.465E-03	11.2
525. - 490.	0.204E-03	7.0	0.297E-03	6.6	0.628E-03	9.1	0.692E-03	12.8
490. - 470.	0.290E-03	8.2	0.381E-03	8.7	0.778E-03	10.9	0.942E-03	9.5
470. - 450.	0.242E-03	8.2	0.400E-03	7.8	0.687E-03	14.1	0.942E-03	13.5
450. - 430.	0.272E-03	7.2	0.357E-03	7.8	0.904E-03	8.5	0.991E-03	9.6
430. - 410.	0.251E-03	8.6	0.462E-03	7.7	0.904E-03	12.4	0.954E-03	9.9
410. - 390.	0.272E-03	8.8	0.469E-03	6.8	0.103E-02	10.8	0.734E-03	15.1
390. - 370.	0.285E-03	8.7	0.429E-03	7.4	0.114E-02	8.2	0.966E-03	12.3
370. - 350.	0.262E-03	8.2	0.512E-03	7.6	0.110E-02	9.5	0.966E-03	9.8
350. - 330.	0.281E-03	7.9	0.443E-03	7.3	0.101E-02	9.5	0.116E-02	9.3
330. - 310.	0.276E-03	8.3	0.465E-03	7.0	0.916E-03	11.4	0.120E-02	9.6
310. - 290.	0.234E-03	9.0	0.426E-03	7.5	0.110E-02	10.5	0.108E-02	8.8
290. - 270.	0.281E-03	7.5	0.409E-03	7.9	0.111E-02	10.5	0.966E-03	10.7
270. - 250.	0.229E-03	9.1	0.479E-03	6.6	0.145E-02	9.0	0.157E-02	10.6
250. - 230.	0.242E-03	8.4	0.496E-03	7.4	0.134E-02	10.4	0.153E-02	7.6
230. - 210.	0.256E-03	7.4	0.448E-03	7.8	0.137E-02	7.3	0.158E-02	9.7
210. - 195.	0.279E-03	8.8	0.473E-03	8.5	0.107E-02	12.7	0.176E-02	10.4
195. - 185.	0.274E-03	12.3	0.498E-03	10.8	0.128E-02	16.5	0.144E-02	13.8
185. - 175.	0.238E-03	12.8	0.579E-03	8.8	0.135E-02	13.8	0.228E-02	11.7
175. - 165.	0.307E-03	9.8	0.493E-03	10.1	0.137E-02	11.7	0.215E-02	11.2
165. - 155.	0.184E-03	13.5	0.378E-03	10.8	0.160E-02	12.9	0.181E-02	11.9
155. - 145.	0.281E-03	11.6	0.503E-03	10.1	0.151E-02	10.9	0.171E-02	11.2
145. - 135.	0.227E-03	11.6	0.556E-03	9.2	0.213E-02	7.7	0.223E-02	8.1
135. - 125.	0.231E-03	13.1	0.412E-03	10.8	0.254E-02	8.9	0.223E-02	14.3
125. - 115.	0.289E-03	11.8	0.527E-03	9.9	0.224E-02	11.1	0.205E-02	10.1
115. - 105.	0.314E-03	11.7	0.618E-03	8.1	0.243E-02	9.7	0.316E-02	10.6
105. - 97.5	0.289E-03	12.5	0.664E-03	9.9	0.299E-02	9.6	0.241E-02	9.9
97.5 - 92.5	0.354E-03	14.1	0.623E-03	12.6	0.183E-02	15.6	0.191E-02	13.9
92.5 - 87.5	0.289E-03	14.2	0.594E-03	12.9	0.270E-02	13.0	0.357E-02	13.4
87.5 - 82.5	0.303E-03	16.3	0.556E-03	11.8	0.266E-02	13.6	0.421E-02	12.1
82.5 - 77.5	0.281E-03	15.4	0.584E-03	13.2	0.307E-02	12.7	0.289E-02	12.3
77.5 - 72.5	0.390E-03	13.3	0.575E-03	12.8	0.394E-02	9.8	0.338E-02	11.7
72.5 - 67.5	0.310E-03	14.9	0.718E-03	11.6	0.302E-02	11.5	0.391E-02	13.2
67.5 - 62.5	0.390E-03	14.8	0.795E-03	11.0	0.352E-02	12.3	0.362E-02	9.1
62.5 - 57.5	0.548E-03	10.8	0.814E-03	9.7	0.417E-02	10.5	0.411E-02	10.5
57.5 - 52.5	0.411E-03	12.5	0.910E-03	11.1	0.394E-02	12.1	0.352E-02	11.4
52.5 - 49.	0.464E-03	15.3	0.111E-02	10.6	0.392E-02	10.9	0.468E-02	15.8
49. - 47.	0.577E-03	16.6	0.862E-03	16.1	0.526E-02	14.8	0.550E-02	12.4
47. - 45.	0.505E-03	19.7	0.113E-02	13.3	0.504E-02	12.8	0.538E-02	16.4
45. - 43.	0.505E-03	17.6	0.108E-02	16.8	0.641E-02	12.9	0.599E-02	11.8
43. - 41.	0.361E-03	22.5	0.982E-03	16.3	0.446E-02	14.8	0.575E-02	14.1
41. - 39.	0.667E-03	14.7	0.110E-02	12.5	0.607E-02	13.3	0.526E-02	16.9
39. - 37.	0.649E-03	15.0	0.117E-02	18.2	0.561E-02	14.4	0.734E-02	12.4
37. - 35.	0.595E-03	19.8	0.910E-03	17.5	0.664E-02	12.4	0.734E-02	10.6
35. - 33.	0.433E-03	21.4	0.108E-02	15.9	0.607E-02	17.8	0.673E-02	17.1
33. - 31.	0.812E-03	14.6	0.127E-02	15.0	0.549E-02	18.1	0.758E-02	12.9
31. - 29.	0.451E-03	20.0	0.148E-02	14.3	0.881E-02	11.5	0.783E-02	11.2

Tab. C-5 : HETC/KFA-2 calculations of double differential cross sections for neutron emission at angles between 6. and 9. degree from targets elements C, Al, Pb and U induced by 800 MeV protons

Incident Energy : 800.MeV

Angle-interval : 6. - 9. degree

Target Elements:	C		Al		Pb		U	
Energy-Bin [MeV]	Cross-section [b/MeV/sr]	FSD [%]	Cross-section [b/MeV/sr]	FSD [%]	Cross-section [b/MeV/sr]	FSD [%]	Cross-section [b/MeV/sr]	FSD [%]
29. - 27.	0.649E-03	17.0	0.141E-02	14.5	0.721E-02	12.0	0.709E-02	15.6
27. - 25.	0.613E-03	19.3	0.125E-02	15.3	0.744E-02	11.9	0.844E-02	10.5
25. - 23.	0.703E-03	14.5	0.156E-02	13.6	0.778E-02	10.0	0.139E-01	8.2
23. - 21.	0.451E-03	20.8	0.182E-02	11.7	0.104E-01	12.9	0.149E-01	8.7
21. - 19.5	0.433E-03	24.2	0.220E-02	15.2	0.157E-01	8.5	0.191E-01	13.0
19.5 - 18.5	0.613E-03	23.7	0.287E-02	15.0	0.121E-01	15.3	0.122E-01	18.5
18.5 - 17.5	0.649E-03	22.9	0.239E-02	15.4	0.130E-01	13.7	0.181E-01	13.9
17.5 - 16.5	0.541E-03	25.7	0.235E-02	17.0	0.160E-01	15.4	0.279E-01	13.1
16.5 - 15.5	0.830E-03	24.6	0.273E-02	16.0	0.133E-01	20.2	0.389E-01	7.1
15.5 - 14.5	0.105E-02	18.5	0.206E-02	16.3	0.128E-01	14.4	0.306E-01	7.2
14.5 - 13.5	0.613E-03	22.2	0.292E-02	13.6	0.199E-01	11.6	0.316E-01	10.1
13.5 - 12.5	0.721E-03	23.6	0.249E-02	15.1	0.215E-01	10.4	0.401E-01	7.5
12.5 - 11.5	0.112E-02	17.6	0.340E-02	13.2	0.293E-01	8.9	0.511E-01	6.8
11.5 - 10.5	0.108E-02	18.0	0.326E-02	12.5	0.256E-01	9.4	0.487E-01	5.9
10.5 - 9.75	0.106E-02	21.0	0.313E-02	14.1	0.336E-01	8.6	0.646E-01	5.7
9.75 - 9.25	0.866E-03	27.2	0.259E-02	20.3	0.467E-01	9.1	0.646E-01	9.3
9.25 - 8.75	0.144E-02	23.6	0.345E-02	17.4	0.554E-01	8.8	0.881E-01	8.9
8.75 - 8.25	0.137E-02	28.7	0.402E-02	17.0	0.536E-01	8.5	0.900E-01	6.3
8.25 - 7.75	0.108E-02	23.9	0.412E-02	15.9	0.508E-01	11.0	0.101E+00	6.4
7.75 - 7.25	0.152E-02	21.7	0.402E-02	17.0	0.732E-01	7.0	0.104E+00	5.6
7.25 - 6.75	0.115E-02	23.0	0.690E-02	12.5	0.710E-01	6.5	0.131E+00	6.4
6.75 - 6.25	0.152E-02	21.7	0.527E-02	16.0	0.764E-01	8.1	0.126E+00	6.2
6.25 - 5.75	0.144E-02	23.6	0.536E-02	14.4	0.911E-01	8.2	0.184E+00	6.0
5.75 - 5.25	0.209E-02	17.2	0.565E-02	13.4	0.115E+00	8.1	0.199E+00	5.1
5.25 - 4.75	0.159E-02	21.0	0.690E-02	9.5	0.128E+00	5.1	0.225E+00	5.0

Tab. C-5 (cont.) : HETC/KFA-2 calculations of double differential cross sections for neutron emission at angles between 6. and 9. degree from targets elements C, Al, Pb and U induced by 800 MeV protons

Incident Energy : 800.MeV

Angle-interval : 28.5 - 31.5 degree

Target Elements: C Al Pb U

Energy-Bin [MeV]	C Cross-section [b/MeV/sr]	C FSD [%]	Al Cross-section [b/MeV/sr]	Al FSD [%]	Pb Cross-section [b/MeV/sr]	Pb FSD [%]	U Cross-section [b/MeV/sr]	U FSD [%]
800. - 775.	0.000E+00	0.0	0.000E+00	0.0	0.000E+00	0.0	0.000E+00	0.0
775. - 725.	0.113E-05	39.8	0.250E-05	33.3	0.717E-05	38.7	0.511E-05	48.4
725. - 675.	0.527E-05	19.1	0.975E-05	17.8	0.311E-04	17.6	0.332E-04	21.4
675. - 625.	0.203E-04	10.8	0.345E-04	8.0	0.103E-03	12.6	0.792E-04	13.4
625. - 575.	0.477E-04	6.1	0.760E-04	5.8	0.154E-03	8.9	0.170E-03	7.7
575. - 525.	0.804E-04	4.8	0.122E-03	4.9	0.275E-03	7.6	0.309E-03	6.5
525. - 490.	0.716E-04	6.6	0.105E-03	6.2	0.258E-03	8.8	0.312E-03	7.9
490. - 470.	0.513E-04	9.1	0.963E-04	8.5	0.266E-03	11.1	0.307E-03	11.3
470. - 450.	0.499E-04	9.9	0.963E-04	7.0	0.236E-03	13.3	0.220E-03	14.2
450. - 430.	0.414E-04	10.3	0.731E-04	9.2	0.212E-03	10.5	0.224E-03	11.9
430. - 410.	0.405E-04	10.6	0.913E-04	7.5	0.281E-03	10.5	0.224E-03	12.4
410. - 390.	0.551E-04	9.5	0.938E-04	7.3	0.314E-03	10.1	0.361E-03	9.3
390. - 370.	0.659E-04	8.0	0.108E-03	7.1	0.361E-03	8.4	0.338E-03	7.7
370. - 350.	0.772E-04	7.3	0.136E-03	6.8	0.379E-03	10.9	0.370E-03	9.3
350. - 330.	0.885E-04	8.1	0.162E-03	5.2	0.475E-03	6.6	0.453E-03	7.1
330. - 310.	0.108E-03	6.9	0.185E-03	5.4	0.598E-03	6.4	0.677E-03	7.5
310. - 290.	0.116E-03	6.1	0.194E-03	5.4	0.621E-03	6.4	0.703E-03	9.2
290. - 270.	0.135E-03	5.6	0.233E-03	5.0	0.753E-03	7.5	0.801E-03	7.0
270. - 250.	0.148E-03	5.4	0.278E-03	4.9	0.762E-03	6.1	0.766E-03	5.7
250. - 230.	0.171E-03	5.2	0.292E-03	4.6	0.992E-03	6.1	0.993E-03	5.3
230. - 210.	0.164E-03	5.0	0.302E-03	4.3	0.113E-02	5.5	0.118E-02	4.3
210. - 195.	0.151E-03	6.6	0.316E-03	4.8	0.117E-02	5.6	0.135E-02	4.8
195. - 185.	0.169E-03	7.0	0.329E-03	6.3	0.124E-02	6.7	0.135E-02	7.3
185. - 175.	0.182E-03	7.3	0.336E-03	5.9	0.117E-02	6.6	0.156E-02	8.1
175. - 165.	0.176E-03	7.1	0.353E-03	6.7	0.140E-02	7.2	0.133E-02	6.8
165. - 155.	0.211E-03	6.8	0.355E-03	5.8	0.125E-02	7.3	0.159E-02	5.6
155. - 145.	0.199E-03	7.2	0.335E-03	5.3	0.171E-02	6.6	0.188E-02	5.5
145. - 135.	0.184E-03	6.9	0.414E-03	5.8	0.143E-02	6.6	0.159E-02	5.0
135. - 125.	0.209E-03	6.3	0.383E-03	5.1	0.196E-02	5.7	0.218E-02	6.0
125. - 115.	0.202E-03	6.7	0.421E-03	4.5	0.160E-02	5.7	0.201E-02	5.7
115. - 105.	0.190E-03	7.8	0.411E-03	5.1	0.188E-02	6.4	0.235E-02	3.9
105. - 97.5	0.191E-03	7.6	0.403E-03	6.5	0.208E-02	6.8	0.228E-02	5.2
97.5 - 92.5	0.232E-03	9.7	0.483E-03	7.5	0.235E-02	6.7	0.211E-02	7.2
92.5 - 87.5	0.245E-03	8.3	0.440E-03	7.5	0.235E-02	7.7	0.271E-02	6.3
87.5 - 82.5	0.230E-03	8.6	0.515E-03	7.6	0.256E-02	6.4	0.236E-02	6.9
82.5 - 77.5	0.245E-03	7.9	0.483E-03	7.1	0.269E-02	6.1	0.292E-02	8.0
77.5 - 72.5	0.218E-03	8.0	0.463E-03	7.9	0.256E-02	8.0	0.299E-02	6.0
72.5 - 67.5	0.213E-03	10.6	0.483E-03	7.0	0.331E-02	5.8	0.303E-02	6.2
67.5 - 62.5	0.222E-03	9.4	0.500E-03	7.3	0.327E-02	5.5	0.308E-02	6.3
62.5 - 57.5	0.239E-03	9.1	0.520E-03	6.8	0.370E-02	5.8	0.336E-02	6.0
57.5 - 52.5	0.234E-03	9.1	0.570E-03	6.1	0.406E-02	6.8	0.381E-02	6.2
52.5 - 49.	0.261E-03	11.1	0.575E-03	8.4	0.429E-02	6.4	0.401E-02	6.2
49. - 47.	0.170E-03	14.5	0.550E-03	11.0	0.382E-02	8.0	0.418E-02	9.8
47. - 45.	0.268E-03	12.5	0.731E-03	9.6	0.359E-02	9.0	0.393E-02	8.2
45. - 43.	0.278E-03	13.2	0.538E-03	11.3	0.514E-02	5.6	0.508E-02	8.8
43. - 41.	0.259E-03	11.7	0.650E-03	9.3	0.415E-02	7.1	0.581E-02	6.6
41. - 39.	0.250E-03	14.8	0.650E-03	10.6	0.466E-02	7.4	0.485E-02	8.5
39. - 37.	0.320E-03	13.0	0.769E-03	10.1	0.511E-02	7.0	0.559E-02	7.5
37. - 35.	0.259E-03	15.1	0.694E-03	10.1	0.481E-02	7.8	0.581E-02	7.8
35. - 33.	0.311E-03	13.8	0.825E-03	8.2	0.448E-02	7.5	0.651E-02	7.6
33. - 31.	0.344E-03	12.6	0.963E-03	9.7	0.493E-02	8.0	0.543E-02	8.1
31. - 29.	0.372E-03	12.8	0.101E-02	7.4	0.556E-02	8.6	0.747E-02	8.3

Tab. C-6 : HETC/KFA-2 calculations of double differential cross sections for neutron emission at angles between 28.5 and 31.5 degree from targets elements C, Al, Pb and U induced by 800 MeV protons

Incident Energy : 800.MeV

Angle-interval : 28.5 - 31.5 degree

Target Elements:	C		Al		Pb		U	
Energy-Bin [MeV]	Cross-section [b/MeV/sr]	FSD [%]	Cross-section [b/MeV/sr]	FSD [%]	Cross-section [b/MeV/sr]	FSD [%]	Cross-section [b/MeV/sr]	FSD [%]
29. - 27.	0.339E-03	12.0	0.120E-02	8.9	0.699E-02	6.0	0.875E-02	6.8
27. - 25.	0.320E-03	12.7	0.126E-02	8.6	0.505E-02	7.8	0.913E-02	5.2
25. - 23.	0.372E-03	11.6	0.133E-02	8.1	0.795E-02	5.0	0.107E-01	5.9
23. - 21.	0.391E-03	11.8	0.144E-02	7.1	0.887E-02	5.4	0.115E-01	4.6
21. - 19.5	0.452E-03	13.0	0.169E-02	7.1	0.104E-01	7.5	0.146E-01	4.5
19.5 - 18.5	0.546E-03	13.5	0.179E-02	8.8	0.111E-01	10.3	0.179E-01	6.9
18.5 - 17.5	0.518E-03	15.1	0.195E-02	9.8	0.144E-01	6.1	0.204E-01	8.6
17.5 - 16.5	0.527E-03	13.7	0.243E-02	9.3	0.144E-01	6.2	0.207E-01	6.8
16.5 - 15.5	0.678E-03	12.0	0.221E-02	9.0	0.166E-01	7.1	0.257E-01	6.7
15.5 - 14.5	0.593E-03	13.3	0.231E-02	8.3	0.156E-01	6.4	0.290E-01	4.8
14.5 - 13.5	0.631E-03	10.8	0.220E-02	8.0	0.179E-01	6.7	0.312E-01	4.5
13.5 - 12.5	0.631E-03	11.2	0.251E-02	6.9	0.229E-01	4.3	0.404E-01	3.9
12.5 - 11.5	0.678E-03	11.7	0.265E-02	6.3	0.238E-01	4.4	0.422E-01	3.8
11.5 - 10.5	0.791E-03	11.7	0.265E-02	6.1	0.252E-01	3.9	0.492E-01	3.1
10.5 - 9.75	0.866E-03	13.0	0.335E-02	6.8	0.351E-01	4.6	0.601E-01	3.0
9.75 - 9.25	0.904E-03	13.1	0.375E-02	8.2	0.385E-01	5.5	0.770E-01	3.8
9.25 - 8.75	0.923E-03	14.1	0.328E-02	9.3	0.457E-01	4.7	0.826E-01	3.4
8.75 - 8.25	0.113E-02	14.0	0.408E-02	6.7	0.478E-01	4.5	0.874E-01	4.3
8.25 - 7.75	0.109E-02	13.0	0.443E-02	7.0	0.537E-01	4.7	0.108E+00	3.0
7.75 - 7.25	0.119E-02	13.7	0.478E-02	7.0	0.559E-01	5.3	0.110E+00	3.2
7.25 - 6.75	0.107E-02	11.8	0.483E-02	7.0	0.675E-01	4.4	0.142E+00	3.6
6.75 - 6.25	0.111E-02	12.1	0.513E-02	6.7	0.778E-01	3.9	0.142E+00	3.8
6.25 - 5.75	0.128E-02	11.6	0.513E-02	6.8	0.790E-01	3.2	0.167E+00	2.8
5.75 - 5.25	0.179E-02	10.3	0.560E-02	5.4	0.964E-01	3.9	0.190E+00	2.2
5.25 - 4.75	0.156E-02	10.0	0.638E-02	6.2	0.119E+00	3.2	0.209E+00	2.3

Tab. C-6 (cont.) : HETC/KFA-2 calculations of double differential cross sections for neutron emission at angles between 28.5 and 31.5 degree from targets elements C, Al, Pb and U induced by 800 MeV protons